The coupled atmosphere-ocean response to Antarctic sea-ice loss

Article

Accepted Version

The coupled atmosphere-ocean response to Antarctic sea-ice loss

Holly C. Ayres,[a,b] James A. Screen,[b] Edward W. Blockley,[c] Thomas J. Bracegirdle[d].

[a] *Department of Meteorology, University of Reading, Reading, UK*

[b] *College of Engineering, Mathematics and Physical Sciences, University of Exeter, Exeter, UK*

[c] *Met Office Hadley Centre, Met Office, Exeter, UK*

[d] *British Antarctic Survey, Cambridge, UK*

Corresponding author: Holly C Ayres, h.c.ayres@reading.ac.uk

ABSTRACT

Antarctic sea ice is projected to decrease in response to increasing greenhouse gas concentrations. Limited studies so far have examined the coupled atmosphere-ocean response to Antarctic sea-ice loss. Here, we isolate the response to Antarctic sea-ice loss in the atmosphere and ocean using bespoke sea-ice albedo perturbation experiments with HadGEM3-GC31-LL, provide the first detailed examination of the global ocean response, and quantify the importance of atmosphere-ocean coupling, through comparison to uncoupled experiments with prescribed Antarctic sea-ice loss. Lower tropospheric warming and moistening over regions of sea-ice loss and the nearby Southern Ocean are simulated in both coupled and uncoupled configurations but are of greater magnitude in the coupled model. A weakening and equatorward shift of the tropospheric westerly jet are simulated in both configurations, but are also larger in the coupled model. Ocean coupling allows the warming response to spread northward, and by poleward atmospheric energy transport, back to the Antarctic interior. Warmer tropical sea surface temperatures enhance atmospheric convection, driving upper-tropospheric warming and triggering atmospheric teleconnections to the extratropics, including a weakened Aleutian Low. A 20% reduction in Antarctic Circumpolar Current transport and a weakening of the shallow tropical convergence cell are simulated. Surface waters warm and freshen globally, becoming more stratified and stable in the Southern Ocean, with similar changes, but of lesser magnitude, in the Arctic Ocean, where sea ice declines. Our results suggest that the climate effects of Antarctic sea-ice loss stretch from pole-to-pole and from the heights of the tropical troposphere to the depths of the Southern Ocean.

1. Introduction

Over the modern satellite era, from 1979 to 2018, annual-mean Antarctic sea ice extent (SIE) increased, on average, by 11 thousand square kilometres per year (Parkinson, 2019). This counterintuitive increase, in a warming world, contrasts with the large decline in the Arctic, and the decline simulated for the Antarctic in models over the historical period (e.g., Meredith et al., 2019). Many possible explanations for observed increase of Antarctic sea ice cover, and the failure of models to reproduce it, have been suggested, including, but not limited to, internal climate variability (Singh et al., 2019), stratospheric ozone depletion (Turner et al., 2009;

Polvani et al., 2011), and surface freshening due to enhanced precipitation (Liu and Curry 2010) or glacial meltwater (Bintanja et al., 2013; Mackie et al., 2020).

The observed trend of increasing sea ice has become weaker in recent years, and is no longer statistically significant (Parkinson, 2019), after the previous record low SIE in austral winter 2016 (Turner et al., 2017), in addition to a new record low in austral winter 2022 (Raphael & Handcock, 2022). Possible explanations for the sudden 2016 decline include influences from ENSO and an enhanced zonal wavenumber-3 pattern of the westerly jet (Schlosser et al., 2017; Stuecker et al., 2017), a rare stratospheric warming event that subsequently influenced the westerly jet and enhanced ice melt (Meehl et al., 2019; Wang et al., 2019), and the unprecedented opening of a polynya near the Maude Rise (Turner et al., 2020). It is unclear if this substantial reduction is temporary or if the Antarctic sea ice is entering a new era of decline (Ludescher et al., 2018; Eayrs et al., 2021). Regardless, models project Antarctic sea-ice loss over this century in response to increasing greenhouse gas concentrations (Collins et al., 2013; Roach et al., 2020).

The climate response to Arctic sea-ice loss has been well studied (e.g., Blackport & Kushner, 2016; Blackport & Screen, 2020; Cohen et al., 2014; Deser et al., 2015; Kim et al., 2014; Peings & Magnusdottir, 2014; Screen et al., 2018; Screen & Simmonds, 2013; Screen et al., 2013; Vavrus, 2018; Zappa et al., 2018). By comparison however, only a handful of modelling studies have been conducted on the impacts of Antarctic sea-ice loss. Model studies forced by observed sea ice trends suggest that the growth in Antarctic sea ice results in a slight poleward shift of the tropospheric eddy-driven jet and a positive Southern Annular Mode (SAM) anomaly in winter months (Raphael et al., 2011; Smith et al., 2017). Modelling studies, using atmosphere-only model configurations prescribed with projected Antarctic sea-ice loss, have found contrasting results on the impact on the location of the mid-latitude tropospheric eddy-driven jet, but generally agree that there is a reduction in its strength (Bader et al., 2013; England et al., 2018; Kidston et al., 2011; Menéndez et al., 1999). In addition to the impacts on the jet, England et al. (2018) found that the responses to Antarctic sea-ice loss were more vertically confined, of smaller amplitude, and less seasonally variable than the well-studied response to Arctic sea-ice loss.

Ayres and Screen (2019) provided the first multi-model analysis of the atmospheric response to projected Antarctic sea-ice loss, indirectly inferred from the Coupled Model Intercomparison Project phase 5 (CMIP5) ensemble (Taylor et al., 2012). Antarctic sea-ice loss

caused a robust weakening of the tropospheric westerly jet and favoured the negative phase of the SAM, of greatest magnitude and robustness in spring and summer. In these regards, the response to sea-ice loss acts to weakly damp the strengthening westerly jet and positive SAM responses to increased CO_2. The SAM response to sea-ice loss primarily reflected a reduction in jet strength and to a lesser extent, an equatorward shift in the jet. In spring, this study found multi-model evidence for a weakening polar stratospheric vortex and coupling between the stratospheric and tropospheric zonal wind responses. Sea-ice loss induced warming in the lowermost atmosphere over the high-latitude Southern Ocean, but this warming did not penetrate over the Antarctic continent, consistent with England et al. (2018).

The majority of the above-mentioned studies used atmosphere-only models, as opposed to fully coupled atmosphere-ocean models, which may lead to muted responses, or in the case of Ayres and Screen (2019), used an indirect method that may miss aspects of the remote response. An important role of ocean coupling in the atmospheric response to Arctic sea-ice loss has been established (Deser et al., 2016; Smith et al., 2017; Tomas et al., 2016). Atmosphere-only models depict locally confined changes in response to Arctic sea-ice loss, as far south as the mid-latitudes, whereas coupled models suggest more widespread effects, reaching the tropics and even into the Southern Hemisphere (e.g., Blackport and Kushner 2016; Deser et al., 2016, 2015; Oudar et al., 2017).

Much less is known about the importance of ocean-atmosphere coupling for the response to Antarctic sea-ice loss. England et al., (2020a) was the first study to use a coupled climate model to assess the impact of Antarctic sea-ice loss and showed that ocean dynamics are important in capturing the global response to Antarctic sea-ice loss, just as is the case for the response to Arctic sea-ice loss. These authors found that the tropical response to Antarctic sea-ice loss is like that to Arctic sea-ice loss, particularly in the eastern equatorial Pacific. Antarctic sea-ice loss induced a ‘mini global warming’ signal, having a spatial pattern like that seen in response to increased greenhouse gas concentrations, but with smaller magnitude (this ‘mini global warming’ pattern has also been found in coupled models forced by projected Arctic sea-ice loss). Arctic warming in response to Antarctic sea-ice loss, was induced through changes in tropical Pacific Ocean and associated atmospheric teleconnections to the Aleutian Low (England et al., 2020b). The above two studies suggest that the ocean may play an important role in the climate response to Antarctic sea-ice loss. Yet, the impact of Antarctic sea-ice loss on the ocean has not been assessed in any detail.

Here, we advance the science on the climate response to Antarctic sea-ice loss in three main ways. First, we use a novel coupled modelling framework to isolate the atmospheric response to Antarctic sea-ice loss in the coupled climate system, building on the work of England et al. (2020a; 2020b), and assess the local and global effects. Second, we provide the first detailed examination of the oceanic response to Antarctic sea-ice loss (Section 3f - h). Third, by contrasting analogous coupled and uncoupled experiments, we provide the clearest yet determination of the role of the ocean and atmosphere-ocean coupling in the climate response to Antarctic sea-ice loss.

2. Methods

a. Model configurations

The bespoke sea ice perturbation experiments use the HadGEM3-GC3.1-LL low resolution (N96-ORCA1) global coupled model configuration, which participated in phase 6 of the CMIP (Williams et al., 2017). The model uses the MetUM GA7.1 global atmosphere and JULES GL7.0 land surface configurations (Walters et al. 2017), coupled to the NEMO GO6.0 ocean (Storkey et al., 2018), and CICE GSI8.1 sea ice (Ridley et al., 2018) model configurations. This version has an atmosphere with 85 vertical levels and horizontal resolution of ~135 km at mid-latitudes (N96). The ocean model used has 75 vertical levels with a 1° horizontal resolution on a tripolar grid. An advantage of using the N96-ORCA1 model over the N216-ORCA025 model, is that it requires an order of magnitude less computing power per model year, yet maintains almost the same quality in representation of the global climate (Kuhlbrodt et al., 2018), and, for this study in particular, performs better for Antarctic sea ice (Andrews et al., 2020). The 1° ocean resolution requires a parameterization for eddy-induced transports (Kuhlbrodt et al., 2018; Storkey et al., 2018), which here is a globally uniform coefficient. For the atmosphere-only experiments, the same atmosphere and land component models are used, but are not coupled to either an ocean or sea ice component model, as discussed in section 3c.

b. Coupled experiments

The control experiment was the CMIP6 ‘Preindustrial Control’ simulation (Eyring et al. 2016) of HadGEM3-GC3.1-LL, which was spun-up using CMIP6 Preindustrial forcing (Menary et al., 2018). The version of HadGEM3 used here includes the impact of melt ponds;

ponds are evolved within the sea ice component but only used within the albedo scheme. In the sea ice perturbation experiment, sea-ice loss was induced in the Southern Hemisphere alone, via an albedo perturbation method. More specifically, all sea ice in the Southern Hemisphere was set to have the albedo of a melt pond with 30 cm depth. This perturbation caused an abrupt reduction in sea ice albedo, leading to the increased absorption of shortwave radiation and thus, abrupt Antarctic sea-ice loss. All other forcings were kept constant at preindustrial levels. Although melt ponds are naturally rare in the Antarctic due to thick snow cover (Scott and Feltham 2010), modifying the melt pond scheme was an effective way to control the sea ice in one hemisphere and not the other. All the parameters used within the albedo scheme, i.e., melt-ponds, bare sea ice, and snow, remain globally consistent and unchanged from the control experiment. We use the fact that the albedo of melt-ponds is lower than ice and snow to reduce the total albedo of the sea ice.

Within HadGEM3 the total albedo of the sea ice is calculated, separately for both visible (< 700 nm) and near-infrared (> 700 nm) wavelengths, as a combination of the albedos of bare ice, snow and melt pond using the CCSM3 scheme (Ridley et al., 2018). The evolution of melt pond area fraction, $f_p(n)$, and depth, $h_p(n)$, for ice in thickness category n, are calculated in CICE using the topographic melt pond formulation (Flocco et al., 2010; Hunke et al., 2015). This melt pond scheme includes the evolution of refrozen lids (Flocco et al., 2010), the impact of which are included by using the 'effective pond fraction' within the albedo calculations. When pond depth is less than 4mm, the melt pond has no impact on the albedo for that ice thickness category n, such that the ponded ice albedo is equal to that of bare ice, α_i. Conversely, where melt pond depth is greater than 20 cm, the bare ice albedo has no impact, and the ponded ice albedo is equal to that of a melt pond, α_p. For melt pond depths between these two values, the ponded ice albedo is a function of the underlying bare ice albedo and the pond albedo (Ridley et al., 2018; Briegleb & Light, 2007):

$$\alpha_{p_i}(n) = \frac{h_p(n)}{0.2}\alpha_p + \left(1 - \frac{h_p(n)}{0.2}\right)\alpha_i \quad (1)$$

The total grid-box albedo, $\alpha(n)$, of each sea ice thickness category n, is calculated as the combined ponded ice albedo, $\alpha_{pi}(n)$, bare ice albedo $\alpha_i(n)$, and snow albedo, $\alpha_s(n)$, weighted by the melt pond fraction $f_p(n)$ and snow fraction $f_s(n)$:

$$\alpha(n) = f_p(n)\alpha_{p_i}(n) + \left(1 - f_p(n)\right) \times \left(f_s(n)\alpha_s(n) + \left(1 - f_S(n)\right)\alpha_i\right) \quad (2)$$

Equation (2) dictates that when the melt pond fraction is one, the total albedo is solely dependent on the ponded ice albedo, whereas when melt pond fraction is zero, the total albedo is solely dependent on the snow albedo and bare ice albedo. For the purposes of this work, the melt pond fraction and depth used within the albedo scheme were set to constant values F_p and H_p, imposed as additional model parameters, to control the albedo of the sea ice.

Various combinations of F_p and H_p were tested in short sensitivity experiments, which yielded varying magnitudes of sea-ice loss. Here, we present results using F_p = 1 and H_p = 30 cm. This parameter set resulted in the largest sea ice loss and was chosen to maximise the signal-to-noise ratio and because it gave magnitudes of winter sea-ice loss to be closer to that projected at the end of the twenty-first century (Roach et al., 2020). This forcing was applied continually in a 300-year perturbation simulation, sufficiently long to allow the ocean circulation to reach a new quasi-equilibrium state (Deser et al., 2016).

c. Atmosphere-only experiments

In the uncoupled control simulation, both the prescribed sea ice concentrations and sea surface temperatures were taken from the coupled control simulation, averaged over years 50-300. In the uncoupled sea ice perturbation experiment, sea ice concentrations in the Southern Hemisphere were taken from the coupled albedo perturbation experiment, averaged over years 50-300, whilst those in the Northern Hemisphere were taken from the coupled control simulation. Sea surface temperatures were set to the values from coupled albedo perturbation experiment over regions of Antarctic sea-ice loss, but to the values from the coupled control simulations elsewhere. All external forcings were kept constant at preindustrial levels.

The atmosphere-only simulation were run following the Polar Amplification Model Intercomparison Project protocol (Smith et al., 2018). More specifically, the model was run for 14 months, starting 1st April, with a total of 200 members, whereby the initial conditions are the same, but differ in the initial seed for the stochastic physics scheme. The first 2 months of each run were discarded, and the remaining 200 years averaged to minimise the impact of internal variability.

d. Diagnostics and statistics

Quasi-equilibrated responses were estimated by subtracting the time-mean in the control simulation from that in the perturbation simulation, each comprising 250 years in the coupled

experiments and 200-year ensemble mean in the atmosphere-only experiments. Transient responses in the coupled experiment were estimated by subtracting the control from the perturbation at each time step. The statistical significance of the response (i.e., the difference in means between the control and perturbation experiments) was calculated with the Student's t-test and is reported at the 95% confidence level. All figures display only significant results.

The mid-latitude tropospheric eddy-driven jet was characterised in terms of its strength (the maximum velocity) and latitude, following the methodology used by Ceppi et al. (2018), Zappa et al. (2018) and Ayres and Screen (2019). The Antarctic Circumpolar Current (ACC) volume transport was calculated as the vertically integrated volume transport across Drake Passage (54.5– 61 °S, 61 °W). Sea ice area was calculated by multiplying the sea ice fraction of each grid cell by the true area of each grid cell, and summing over the hemisphere of interest, and has units of (million) square kilometres.

3. Results

a. Sea ice and surface fluxes

Annual-mean Antarctic sea ice area (SIA) is around 13 million km^2 in the coupled control simulation, with a small downward drift over time (Figure 1a). Following the albedo perturbation, SIA decreases to around 8 million km^2 in year 5, and then to around 7 million km^2 by year 20. After this, SIA continues to decrease slowly to 6 million km^2 in year 300. After approximately year 20, the control and perturbed simulation show similar slow rates of decline, such that the anomaly (perturbation minus control) remains fairly level at -6 million km^2 from year 20 to 300, but with interannual and (multi-)decadal variability (Figure 1b). The coupled perturbed simulation exhibits a complete loss of sea ice in summer and a 40% loss in SIA in winter, relative to the preindustrial control state (Figure 1c). The seasonal cycle of SIA loss in real terms (i.e., in square kilometres) is largest in early summer, when the effect of the albedo change is largest, owing to maximum incoming solar radiation, and smallest in late summer, when there is little sea ice in the control run anyway (Figure 1d). The annual-mean sea-ice loss is broadly comparable to that projected in the high emission scenarios by the end of the 21st century, albeit with greater ice loss in the summer and lesser ice loss in winter (not shown).

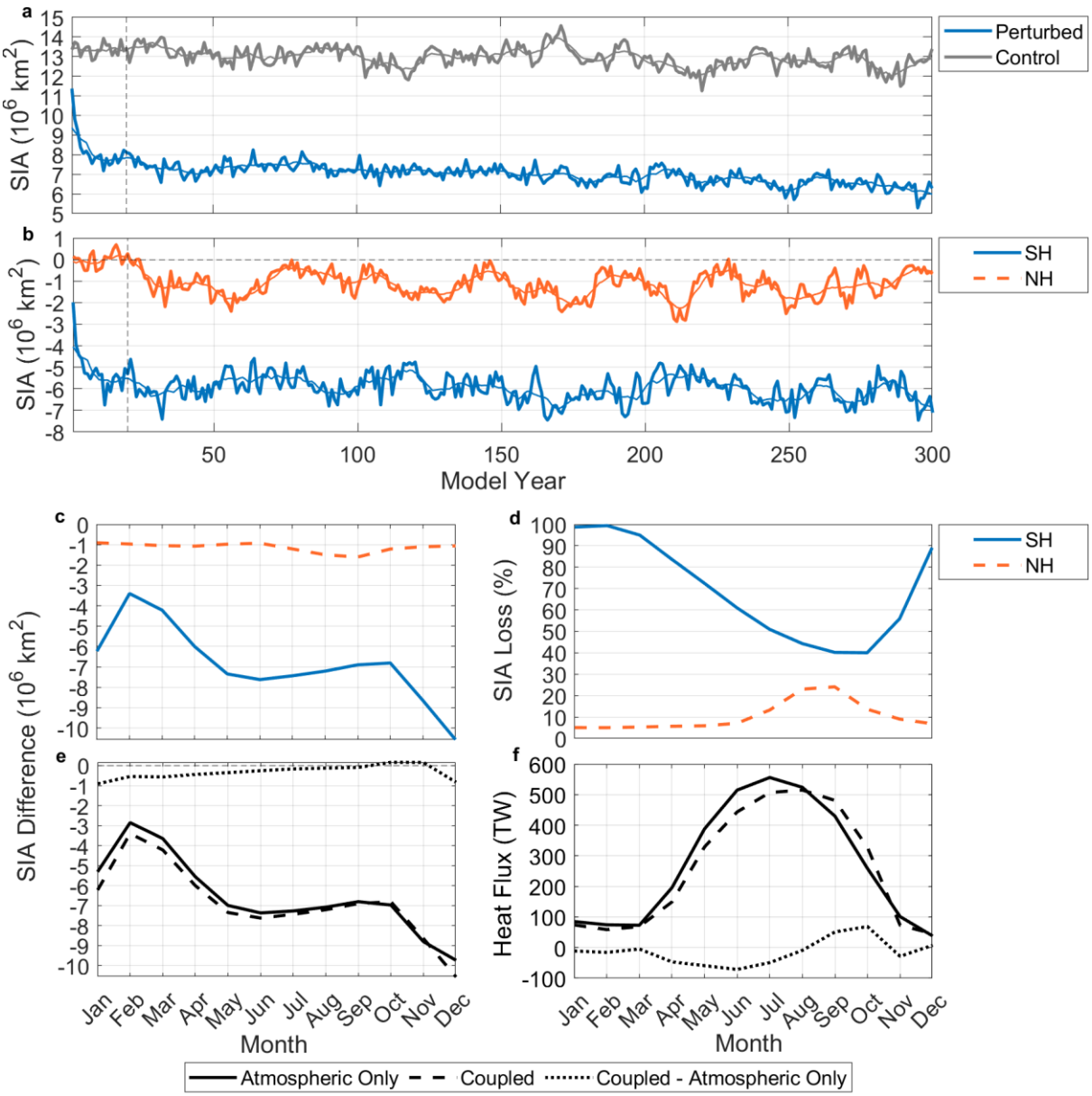

Figure 1. Time-series of Antarctic sea ice area in the coupled control and albedo perturbation experiments (grey and blue, respectively). The thin curves show 10-year running means. The dashed vertical line shows the end of the spin-up period. (b) Time series of sea ice area loss (perturbed minus control) in the Southern and Northern Hemispheres (blue and orange, respectively). (c) Mean annual cycle over the period of 300 years of monthly-mean sea ice area loss (perturbed minus control) in the Southern and Northern Hemispheres (blue and orange, respectively). (d) Annual cycle of monthly-mean percentage sea ice area loss in the Southern and Northern Hemispheres (blue and orange, respectively). (e) Annual cycle of monthly-mean sea ice area change (perturbation minus control) in the coupled and atmosphere-only experiments, and their difference (dashed, solid and dotted lines, respectively). (f) Annual cycle of monthly-mean turbulent heat flux change (perturbation minus control) in the coupled and atmosphere-only experiments, and their difference (dashed, solid and dotted lines, respectively). The heat flux is multiplied by the true area of each grid-box and summed over the grid-boxes where Antarctic sea ice cover is reduced.

This seasonal cycle of ice loss, skewed towards summer, is a characteristic of albedo reduction experiments, which disproportionally reduce sea ice in summer when incoming solar radiation is at its maximum (Sun et al. 2020). One advantage of this approach is that energy, freshwater and salt are conserved, unlike with nudging methods (Screen et al. 2018; Sun et al. 2019).

Although the albedo was only changed in the Southern Hemisphere, Arctic SIA shows 24% loss in boreal summer and 5% loss in boreal winter (Figure 1d), which, although considerably lesser in magnitude than in the Southern Hemisphere, demonstrates a marked reduction of Arctic sea ice in response to Antarctic sea-ice loss. The Arctic sea ice response is delayed by approximately twenty years compared to the imposed sea ice reduction in the Antarctic (Figure 1b), which suggests that the pole-to-pole response may be governed by slow oceanic processes, a concept returned to later.

Recall, sea ice fields from the coupled model were prescribed in the atmosphere only experiments. Figure 1g shows a small discrepancy between the Antarctic SIA loss in the coupled and uncoupled cases, which arises because the atmospheric model (when run in uncoupled mode) replaces sea ice concentrations below 30% with zeros. Further, we note differences in sea ice thickness between the coupled and uncoupled cases (not shown), as in the latter, sea ice thickness is derived empirically from the sea ice concentration and not explicitly simulated. Despite these differences in sea ice states, the heat flux responses are very similar in the coupled and uncoupled cases (Figure 1h), meaning it is appropriate to interpret differences in the atmospheric response between coupled and uncoupled cases as arising due to the coupling and not because of differences in forcing. In both coupled and uncoupled cases, the total turbulent heat flux to the atmosphere peaks in winter at a little over 500 TW and is smallest in summer at less than 100 TW. This seasonal cycle reflects both the magnitude of sea-ice loss in each month and the air-sea temperature difference.

Sea ice concentrations are reduced all year round in the Southern Hemisphere (Figure 2a-d), being of greatest magnitude near the ice edge, which migrates with the seasons. Antarctic sea ice thickness is reduced everywhere within the ice pack in all seasons, except for patches of thickening in summer (Figure 2e-h). In the Arctic, there are modest reductions in sea ice concentration, mostly in the Barents-Kara Sea in boreal winter and spring but extending across the Arctic Ocean in boreal summer and autumn (Figure 2a-d). Sea ice thickness is reduced in all seasons across the Arctic and by similar magnitudes to in the Antarctic (Figure 2e-h). The

spatial patterns of the turbulent (sensible plus latent) heat flux responses largely mimics those of sea ice concentration, with largest increases in the ocean-to-atmosphere heat exchange in regions of ice loss, and seasonally greatest in autumn and winter (Figure 2i-l). Reductions in the turbulent heat flux are seen northward of the sea ice edge in the Southern Ocean, reflecting anomalous heat input. In the Arctic, increased heat fluxes are simulated in the colder boreal season and in regions of reduced sea ice cover, mainly the Barents-Kara Sea.

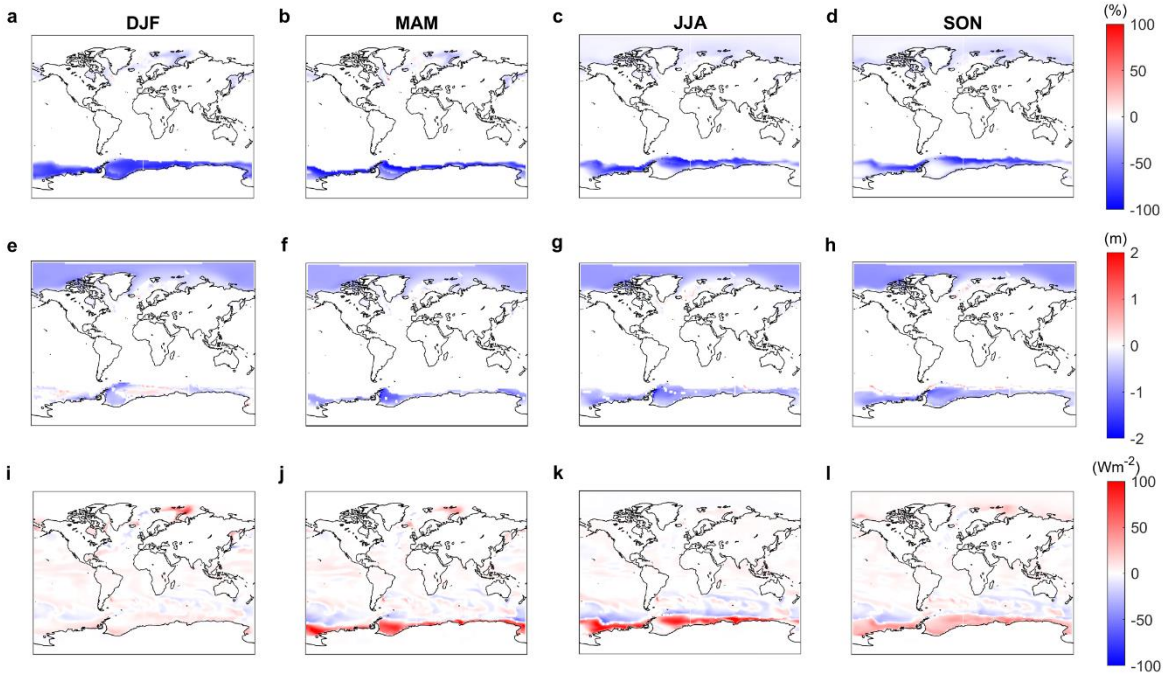

Figure 2. (a-d) Sea ice concentration response, i.e., perturbed minus control, in summer, autumn, winter and spring, respectively. (e-h) As a-d but for sea ice thickness. (i-l) As a-d but for surface turbulent heat flux. The heat flux is defined positive in the upward direction, so red (blue) denotes areas where the heat flux into the ocean is higher (lower) in the perturbed experiments.

b. Spatial pattern of the atmospheric response

The near-surface air temperature response is global in reach in the coupled model, reaching as high as 15 K over regions of Antarctic sea-ice loss in autumn and winter (Figure 3a-d). In polar regions, there is a clear seasonal cycle, with the largest warming in autumn and winter, in each hemisphere, as expected from the heat flux response (Figure 1). An increase in temperature over the Antarctic continent is present in all seasons (Figure 3a-d), with coastal regions warming the most, by up to 5 K in winter and spring, but significant warming extending to the high-altitude plateau in all seasons. There is substantial warming of up to 4 K in the northern regions of the Southern Ocean. Over the tropics, surface warming is similar in each

season, albeit of smaller magnitude than at the poles. In the high latitudes of the Northern Hemisphere, north of 50° N, there is an increase in near-surface air temperature of between 3 K and 8 K, in all seasons apart from boreal summer. The largest increases in near-surface air temperature are in the Barents-Kara Sea in boreal winter, again consistent with the spatial and seasonal pattern of the heat flux response. In the atmosphere-only experiments, the warming is restricted to the regions of sea-ice loss, and the nearby Southern Ocean and coastal regions of the Antarctic continent (Figure 3e-h). Unlike in the coupled experiment, warming does not extend to the high-altitude plateau in any season or north of 50 °S. A highly similar seasonal cycle is seen in the uncoupled and coupled cases, with the largest local warming in autumn and winter, but the maximum warming is ~2 K greater in the coupled compared to uncoupled experiments.

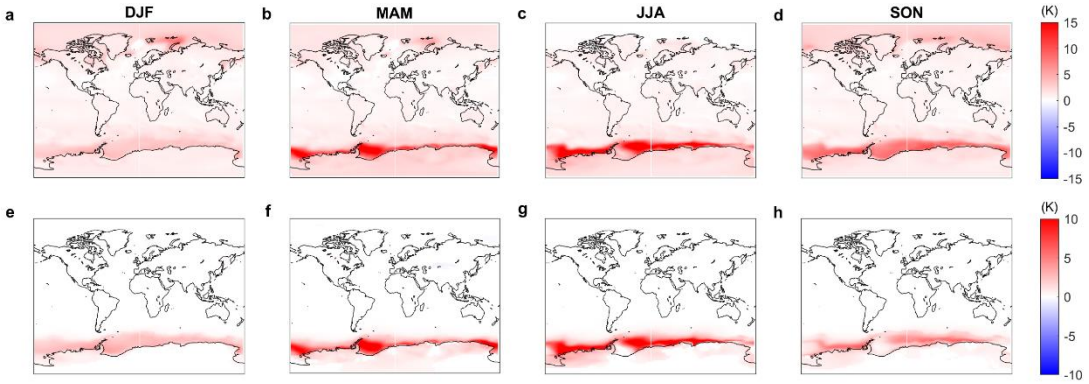

Figure 3. (a-d) Near-surface air temperature response, i.e., perturbed minus control, in austral summer, autumn, winter, and spring, respectively, in the coupled model. (e-h) As a-d but for uncoupled experiments.

In the coupled experiment, the mean sea level pressure (MSLP) response (Figure 4a-d) to Antarctic sea-ice loss shows an increase over Antarctica, up to 2.2 Pa, with the largest and most significant increase in winter. This high-latitude MSLP increase maps onto the negative phase of the SAM. However, the MSLP response over the Southern Ocean is not zonally symmetric. There is a clear weakening of the Amundsen Sea Low from autumn to spring (i.e., increased MSLP), and decreased MSLP in the Weddell Sea in all seasons. North of 50° S, one notable feature is the MSLP decrease over the North Pacific, reflecting a strengthened Aleutian Low in boreal winter and spring. In the uncoupled experiments, there is a decrease in pressure of up to 3 Pa over the Southern Ocean and Antarctic continent in all seasons apart from autumn, when there is a slight increase at the highest latitudes and in the Amundsen Sea Low region (Figure 4e-h). Few regions beyond the Southern Ocean show a significant MSLP response in the uncoupled experiments, with perhaps the exception of winter, when there are patchy MSLP

increases over mid-latitudes. The MSLP responses in the coupled and atmosphere-only models are of opposite sign in many regions, including over Antarctica and in the Amundsen Sea Low region. Broadly speaking, the MSLP response in the uncoupled model is characterised by reduced MSLP in regions of sea-ice loss, a direct "heat low" type response, whereas the coupled model response bears closer resemblance to the negative SAM phase.

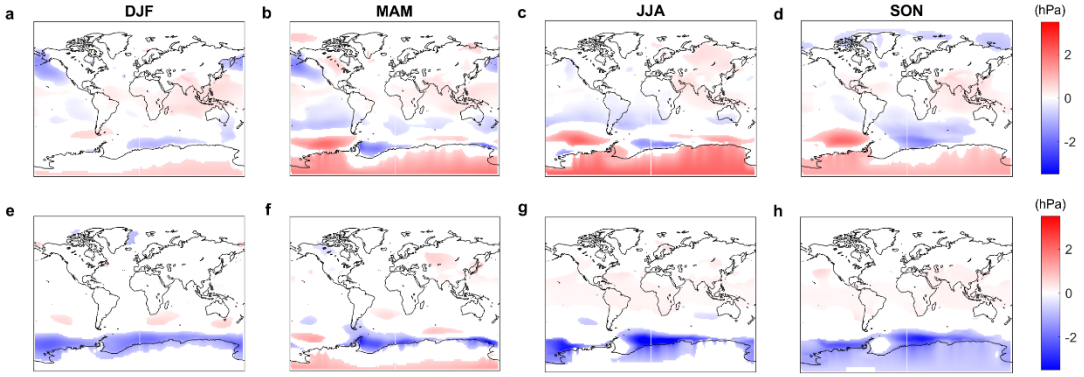

Figure 4. (a-d) Mean sea level pressure response, i.e., perturbed minus control, in austral summer, autumn, winter, and spring, respectively, in the coupled model. (e-h) As a-d but for uncoupled experiments.

The zonal wind response at 500 hPa (U500) (Figure 5a-d) displays a decrease over the latitudes of the westerly jet in all seasons in the coupled model, suggesting a weakening of the jet, which is largest in autumn and winter. The maximum decrease, in winter, amounts to a ~10 % reduction in the mean westerlies. The increase of the equatorward flank of the westerly is less significant. A similar decrease of the zonal wind in the latitudes of the westerly eddy-driven jet is seen in the uncoupled simulation, but of weaker (less than 50% of the magnitude in the coupled mode) magnitude, especially in the warmer seasons, and significant in only autumn and winter (Figure 5e-h). Thus, the weakened westerly response is seen year-round in the coupled model, but only during the colder seasons in the atmosphere-only model. The weakening is also more latitudinally confined in the atmosphere-only model response. In the Northern Hemisphere midlatitudes there is a dipole in the coupled model, suggesting an equatorward shift of the eddy-driven jet, particularly in the Pacific sector in boreal winter and spring. This feature is absent in the uncoupled experiments, which show only small, patchy regions of significant change in the Northern Hemisphere.

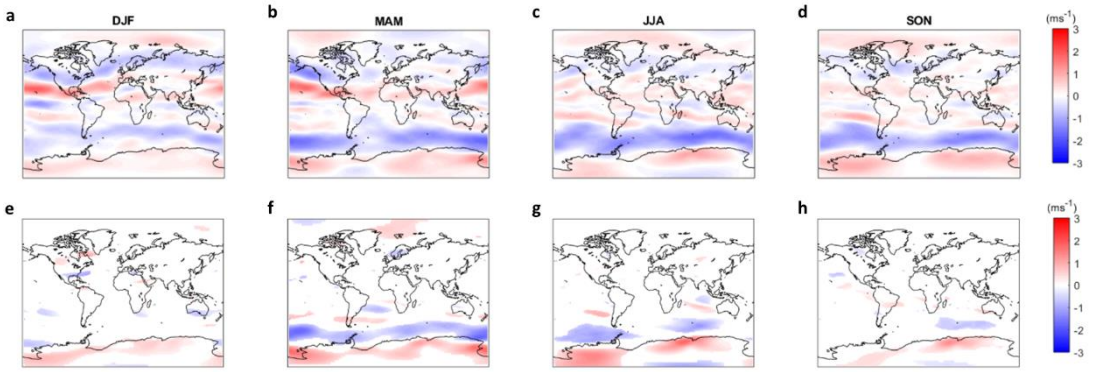

Figure 5. (a-d) 500 hPa zonal wind response, i.e., perturbed minus control, in austral summer, autumn, winter, and spring, respectively, in the coupled model. (e-h) As a-d but for uncoupled experiments.

Precipitation (Figure 6a-d) significantly increases over areas of Antarctic sea-ice loss and the surrounding Southern Ocean, most strongly in autumn and winter, in both coupled and uncoupled experiments. However, the wetting signal is seen over larger swathes of the Southern Ocean in the coupled model, whereas it is locally confined to the higher latitudes in the atmosphere-only model. This greater spatial extent of the wetting signal in the coupled model, compared to that in the atmosphere-only model, is likely due to the more widespread warming (Figure 6e-h) in the coupled model, which is expected to increase moisture availability. Over the Antarctic continent in the coupled model, there is an increase of up to 0.5 mm/day in the coastal regions, with higher latitudes and altitudes seeing a smaller but still significant increase in all seasons. However, there is no significant response over the continent in the uncoupled experiments. A small increase in Arctic precipitation is simulated in boreal autumn and winter, only in the coupled experiments where Arctic sea-ice is reduced.

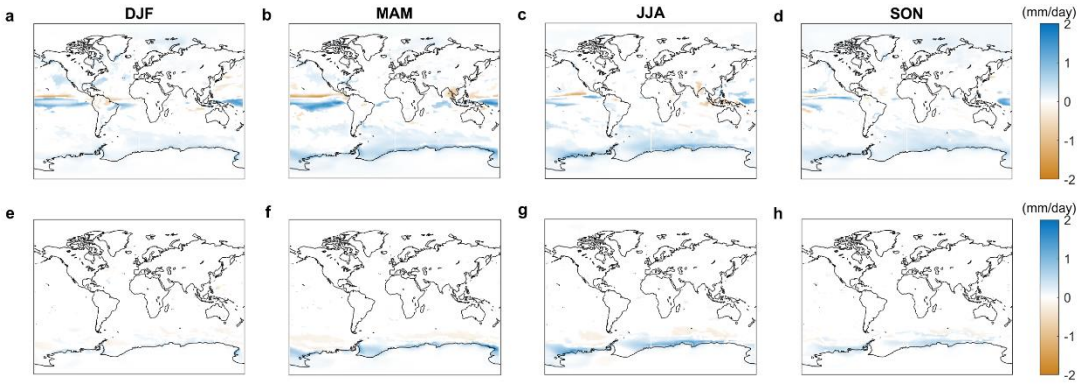

Figure 6. (a-d) Precipitation response, i.e., perturbed minus control, in austral summer, autumn, winter, and spring, respectively, in the coupled model. (e-h) As a-d but for uncoupled experiments.

Precipitation changes in the tropics are also only found in the coupled model and are worthy of closer examination. The annual-mean precipitation response over the tropical Pacific shows a decrease in a band north of the equator, which is climatologically wetter, and an increase along the equator, which is climatologically drier (Figure 7a,b). This suggests a shift of the Intertropical Convergence Zone (ITCZ), analogous but of smaller magnitude to that simulated in response to increased greenhouse gas concentrations (Collins et al. 2013). The spatial pattern of the tropical precipitation response resembles that of SST, with increased precipitation in regions of greater ocean surface warming, relative to the global mean, and reduced precipitation in regions of lesser ocean surface warming, again relative to the global mean (Figure 7c; the "warmer gets wetter" paradigm). Locally enhanced surface warming along the equator in the Pacific Ocean is likely related to reduced upwelling of colder water from depth. Figure 7d show the tropical upper ocean convergence cell in the control run. Upwelling along the equator is balanced by off-equatorial downwelling. In response to Antarctic sea-ice loss, the tropical convergence cell is weakened (Figure 7e), related to the weakened easterly trade winds (Figure 7d)

c. Vertical structure of the atmospheric response

In the coupled model, the zonal-mean temperature response to Antarctic sea-ice loss displays warming throughout the troposphere, with the biggest increase over the high southern latitudes in the lower troposphere (Figure 8a-d). In the upper troposphere, there is a warming at lower latitudes, akin to a classical global warming temperature signature. The stratosphere cools in the Southern Hemisphere, in all seasons apart from winter. In contrast, the Northern Hemisphere stratosphere warms in all seasons apart from boreal autumn. In the absence of ocean coupling, the zonal-mean temperature response displays lower tropospheric warming (up to 500 hPa) over Antarctica and the Southern Ocean, of greatest magnitude in autumn and winter (Figure 8e-h). Although both model versions depict tropospheric warming over the Antarctic and Southern Ocean, this warming is of greater magnitude and extends to higher altitudes in the coupled model. Warming reaches the tropopause over the Antarctic (250 hPa) in the coupled model, whereas it is confined to below 500 hPa in the atmosphere-only model. The Southern Hemisphere polar stratospheric cooling is also of greater magnitude in the coupled model; in fact, this region warms in autumn and winter in the uncoupled case. There is a clear global tropospheric warming signature in the coupled model, which is not present in

the atmospheric-only model. The tropical upper tropospheric warming and Arctic lower tropospheric warming seen in the coupled model response are absent from the atmosphere-only model response.

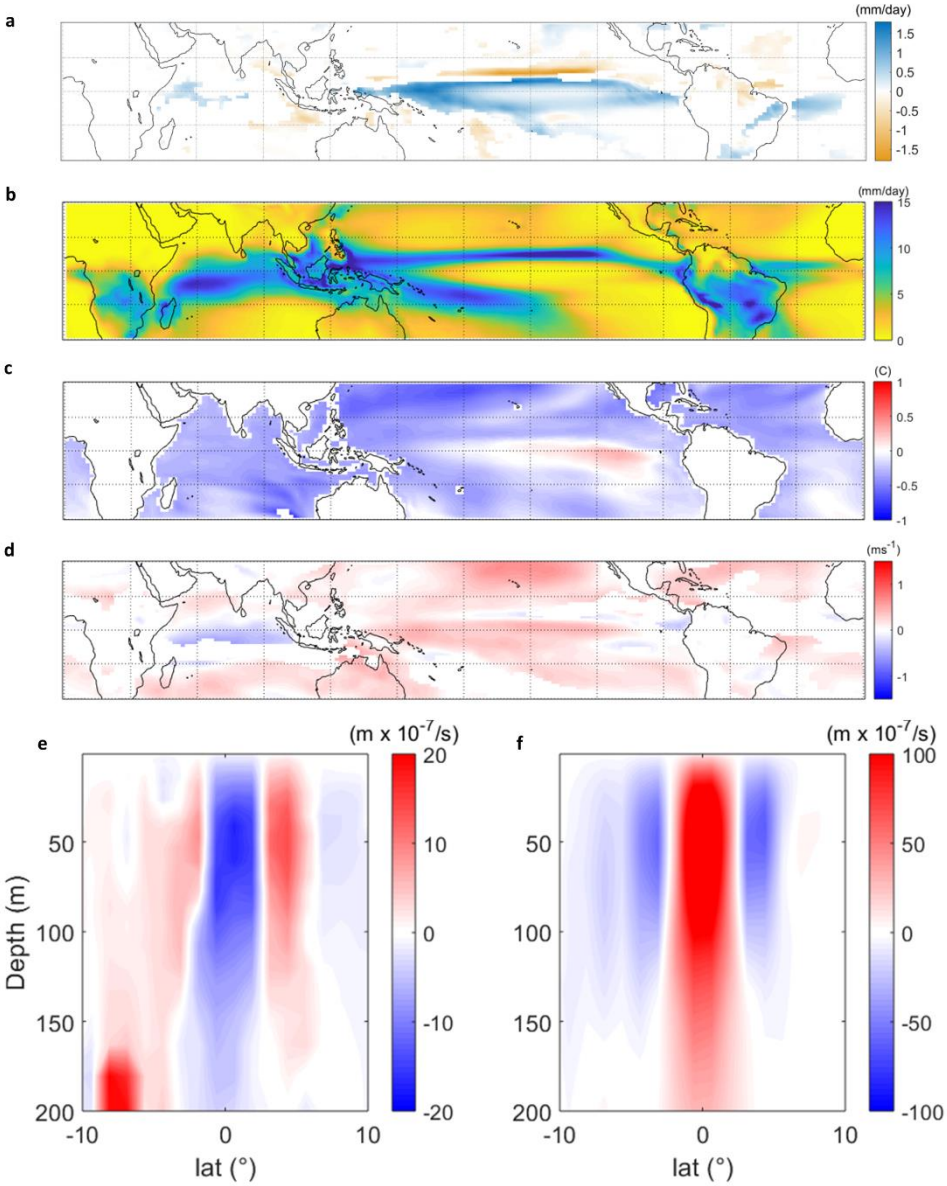

Figure 7. (a) Annual-mean tropical precipitation response, i.e., perturbed minus control, in the coupled model. (b) Annual-mean tropical precipitation in the coupled control simulation. (c) As a but for sea surface temperature. Here, local changes are plotted relative to the global mean response. (d) As a but for zonal wind. (e) Zonal-mean tropical Pacific vertical ocean velocity in the top 200m in the coupled control run. (f) Zonal-mean tropical Pacific vertical ocean velocity response.

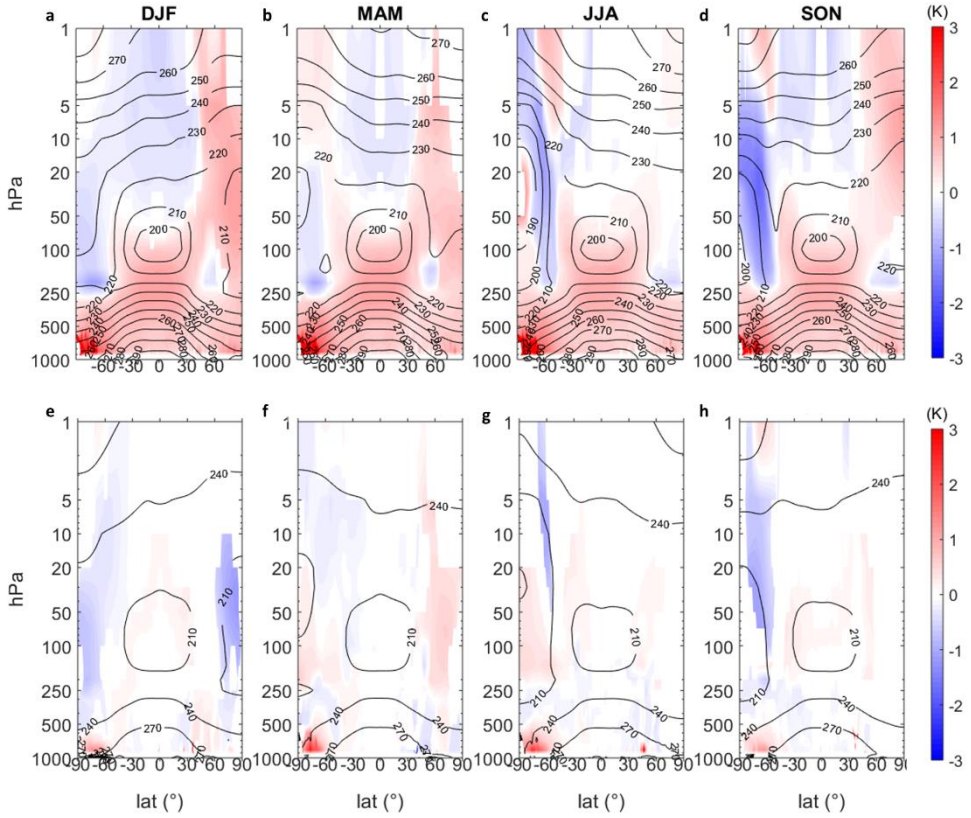

Figure 8. (a-d) Zonal-mean air temperature response, i.e., perturbed minus control, in austral summer, autumn, winter, and spring, respectively, in the coupled model. (e-h) As a-d but for uncoupled experiments.

Turning now to the zonal-mean zonal wind response (Figure 9), the velocities decrease in the core and on the poleward flank of the Southern Hemisphere westerly jet, suggesting a weakening and slight equatorward shift of the jet. This change is seen in all seasons in both the coupled and uncoupled experiments, but is of greater magnitude in the coupled model, especially in the colder seasons. The main differences between the zonal-mean zonal wind responses in the coupled and uncoupled models are in the vicinity of the subtropical jets. In the coupled model, the westerly winds increase in the tropical upper troposphere, in both hemispheres, related to the upper tropospheric tropical warming. These features are absent in the atmosphere-only configuration. Also, in the coupled model only, velocities decrease on the poleward flank of the northern tropospheric eddy-driven jet in boreal winter and spring, suggesting an equatorward shift.

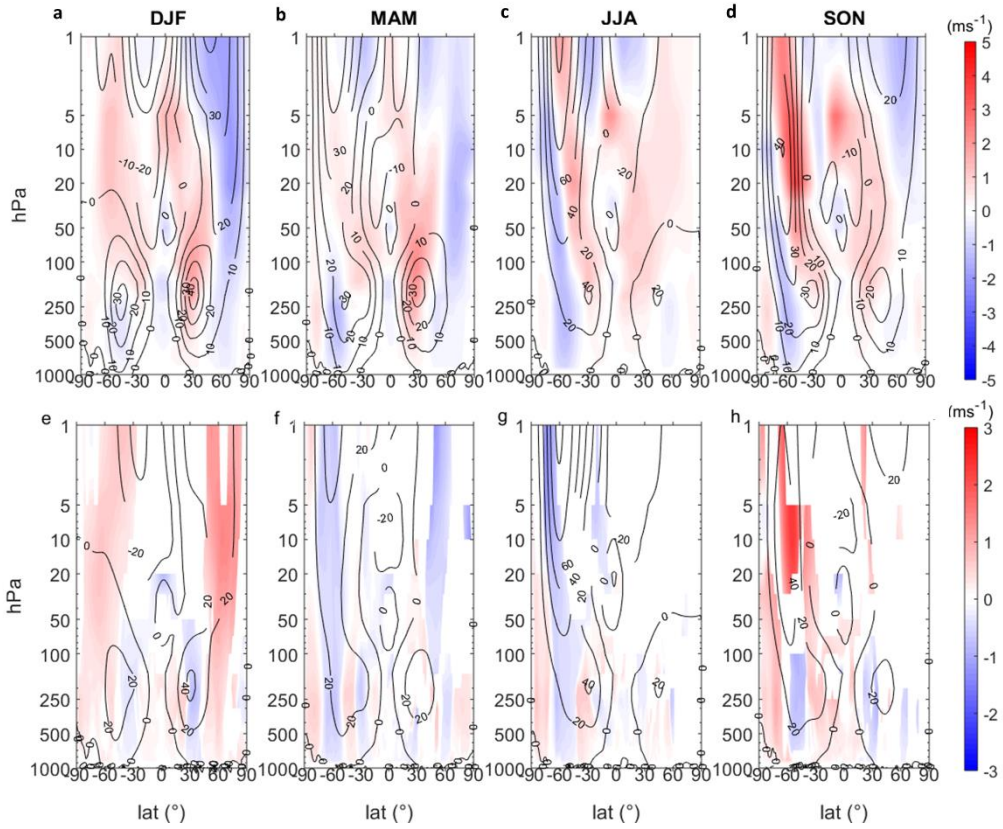

Figure 9. (a-d) Zonal-mean zonal wind response, i.e., perturbed minus control, in austral summer, autumn, winter, and spring, respectively, in the coupled model. (e-h) As a-d but for uncoupled experiments.

d. Responses of the jet streams

The Southern Hemisphere mid-latitude eddy-driven jet shifts equatorward in most months in the coupled model, with a maximum shift of 1.39 ° of latitude in September (Figure 10). A similar jet shift is seen in the uncoupled models during the months March to August, with a maximum of 0.95° in August. The jet weakens throughout the entire year in the coupled model, with maximum weakening of 0.64 ms^{-1} in September, and in most months in the atmosphere-only model, with a maximum weakening in September of 0.3 ms^{-1}. The months of maximum jet weakening broadly correspond to the months with the largest equatorward shifts. Although a robust feature across the two model versions, the jet weakening is of notably greater magnitude in the coupled model than the atmosphere-only model. Ocean coupling appears to be more important for the jet strength response than the jet latitude response to Antarctic sea-ice loss.

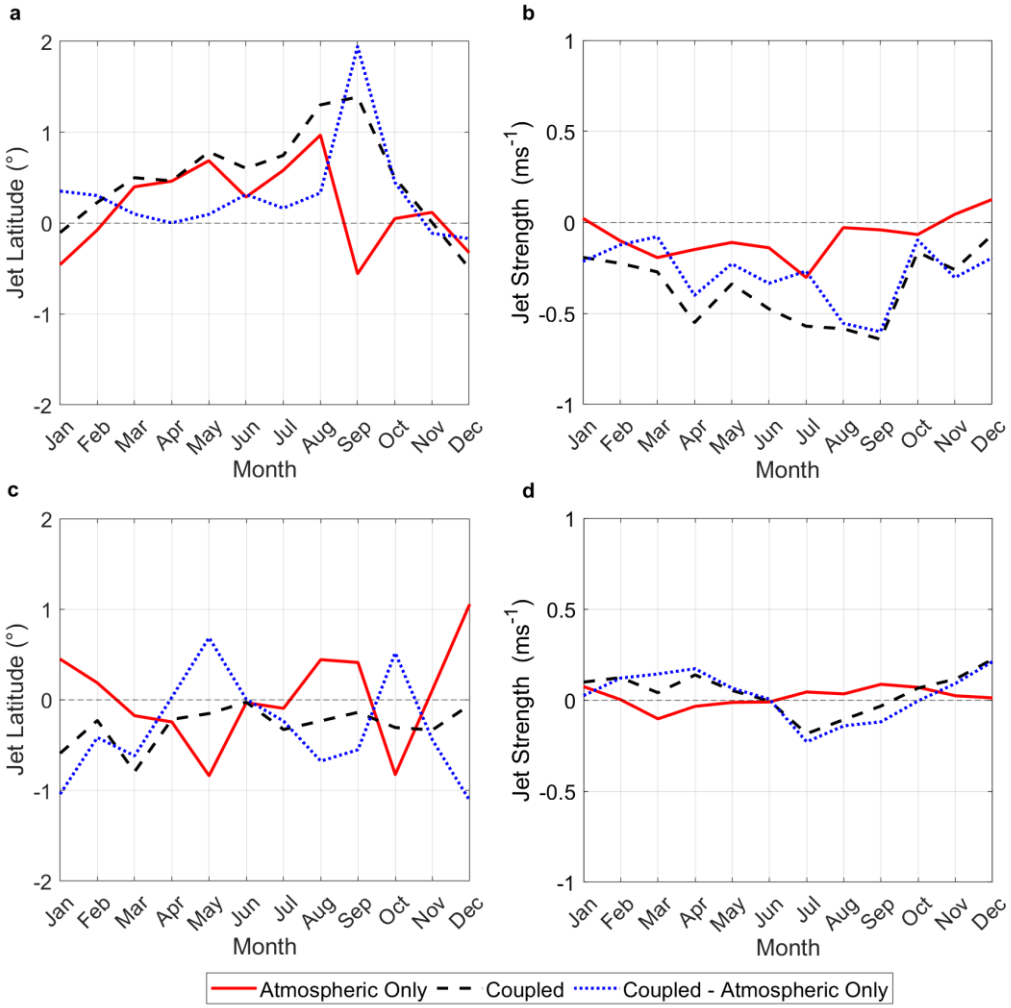

Figure 10. (a) Annual cycle of the monthly-mean response of the Southern Hemisphere eddy-driven jet latitude, in the coupled and uncoupled models and their difference (black, red and blue, respectively). (b) As a but for jet strength. (c-d) As a-b but for the Northern Hemisphere eddy-driven jet.

In the Northern Hemisphere, the eddy-driven jet moves equatorward in all months in the coupled model, with a maximum of 0.79° in March. The jet strength increases in the boreal winter, spring, and autumn, by a maximum of 0.22 ms^{-1} in December, but decreases in boreal summer, with a maximum of 0.18 ms^{-1} in August. Thus, the eddy-driven jets are shifted equatorward in both hemispheres, but the jet weakening is more apparent in the Southern than Northern Hemisphere.

e. Time evolution of the atmospheric response

Surface warming over the Southern Hemisphere extratropics occurs rapidly following the abrupt loss of sea ice, reaching 2 K within 5 years and levelling out around 2.5 K after about 30 years, with small fluctuations due to multi-decadal variability (Figure 11a). In the tropics

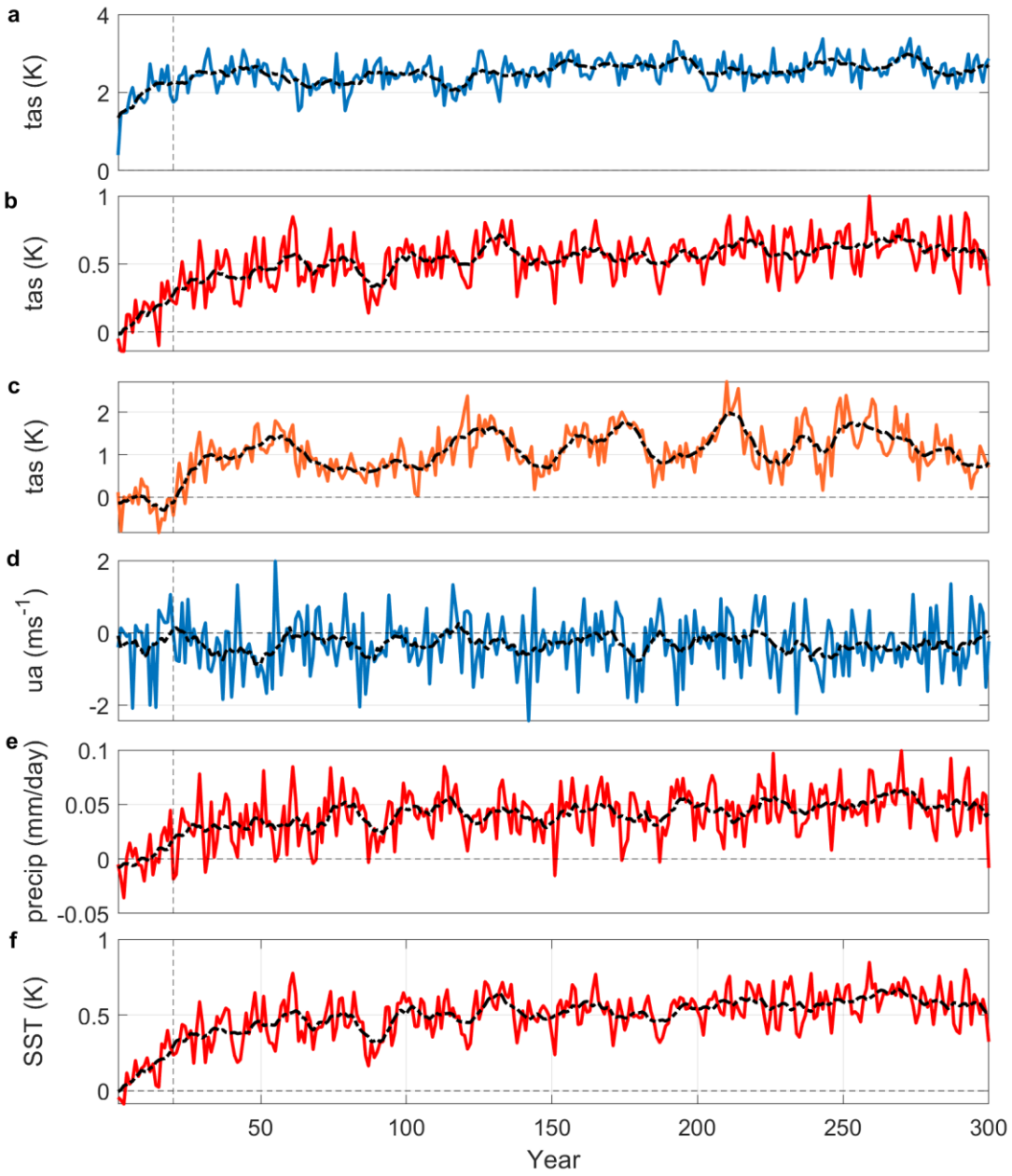

Figure 11. (a) Time series of the annual-mean near-surface air temperature response, i.e., perturbed minus control, averaged over Southern Hemisphere extratropics (70-40 °S). The black line denotes a 10-year running mean, the grey dashed lines denote the 20-year spin-up. (b) As a but averaged over the tropics (30 °N-30 °S). (c) As a but averaged over Northern Hemisphere extratropics (70-40 °N). (d) As a but for 500 hPa zonal wind averaged over the latitude of the westerly jet (65-35 °S). (e) As a, but for precipitation averaged over the tropics (30 N-30 °S). (f) (As a, but for sea surface temperature averaged over the tropics (30 °N-30 °S).

there is a gradual warming over the first 60 years before quasi-equilibrium is reached (Figure 11b). In the Northern Hemisphere extratropics, there is little warming in the first 20 years (Figure 11c). This delay suggests a role for oceanic processes, which evolve more slowly than atmospheric processes. Recall, a similar lag was seen in the Arctic sea ice response (Figure

1b). Warming becomes apparent thereafter, reaching equilibrium after around 60 years (Figure 11c). The Southern Hemisphere tropospheric eddy-driven jet (Figure 11d) exhibits a decrease in the zonal velocity from the beginning of the simulation, consistent with a fast jet weakening response. There is some indication that the jet response lessens after the first seventy years, which might reflect the impact of tropical warming re-establishing a stronger pole-to-equator near-surface temperature difference, but not recovering back to its original state. However, there is substantial internal variability which prevent firm conclusions regarding the transient response. The tropical precipitation and SST responses (Figure 11e,f) follow the same trajectory as tropical surface air temperature (Figure 11b), with a gradual increase over the first 60 years before levelling out. Thus, the tropical air temperature, SST and precipitation responses appear to be governed by similar 'slow' processes, involving the ocean.

f. Surface ocean response

An increase in SST is observed globally in ice-free waters (Figure 12a). In the coastal regions of the Southern Ocean, annual-mean SSTs increase by as much as 4 K, with significant warming extending to the northern regions of the Southern Ocean, up to 40° S. In the tropics and mid-latitudes of both hemispheres, SST increases by approximately 1 K in all ocean basins, with a slightly greater increase in the tropical Pacific than the tropical Atlantic. In the Northern Hemisphere, north of 50° N, there is an increase in SSTs of up to 2 K in the North Atlantic region and Barents-Kara Sea.

A decrease in sea surface salinity in the Arctic Ocean is simulated, with the largest decrease of 1.5 in the Beaufort Sea (Figure 12b). This salinity decrease is an expected result from Arctic sea-ice loss (increased freshwater input and/or reduced brine rejection from ice formation), in addition to the increased precipitation (Figure 6). Surface salinity is increased over the Kara and Laptev Seas in the Arctic, and over the Amundsen and Weddell Seas in the Antarctic. These increases in salinity may relate to changes in advection and mixing, increased evaporation from larger SSTs, in addition to the seasonal melt season. Due to the ice-albedo feedback, sea ice loss is heavily biased towards the summer months, which can lead to more rapid ice formation in autumn and winter, leading to increased brine rejection. Otherwise, decreased sea ice can lead to decreased salinity and brine rejection. The Antarctic is dominated by seasonal ice cover, so the former effect dominates. Regionally, areas of greater seasonal sea ice in the Antarctic show an increase in salinty, whereas regions with more multiyear ice, such as the Weddell Sea, show decreased salinity.

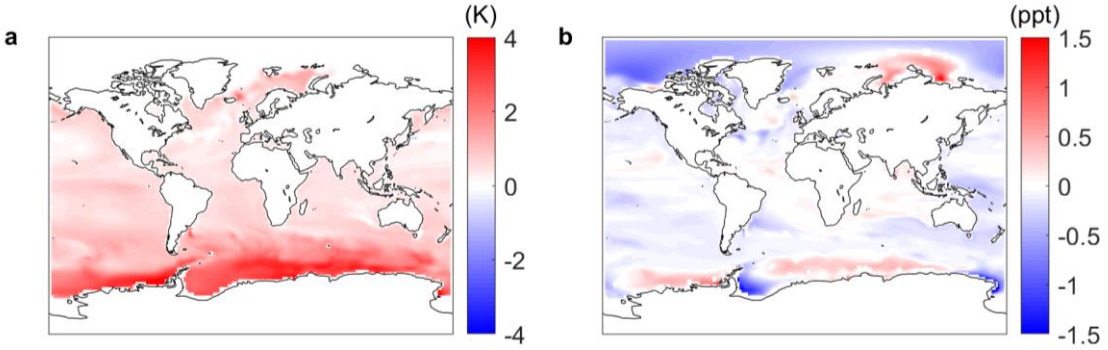

Figure 12: (a) Annual-mean sea surface temperature response, i.e., perturbed minus control. (b) Annual-mean sea surface salinity response.

g. Subsurface ocean response

The zonal-mean temperature response as a function of depth shows warming at all latitudes and depths, suggesting warming of all global water masses (Figure 13a). The overall warming pattern is comparable to that seen in the RCP4.5 scenario (Collins et al., 2013), suggesting that sea-ice loss induces a 'mini global warming' signature in the ocean, analogous to that in the atmosphere. Water in the top 1000 m shows the largest increases, with the greatest warming south of 30° S in all basins, followed by north of 60° N, and then hotspots around the equator. Warming is not limited to the mixed layer, highlighting the role of ocean circulation and mixing in the global response to Antarctic sea-ice loss. In the Southern Ocean, there is marked warming at depth. Antarctic Bottom Water (AABW) is a crucial water mass for the Meridional Overturning Circulation and its temperature increases by up to 1 K (and becomes less dense), potentially reducing downwelling in the region.

Salinity decreases by ~ 0.9 in surface and intermediate waters at most latitudes and increases by ~0.2 in the deep-water masses of the Southern Ocean (Figure 13b). Salinity can be controlled by a variety of factors. The simulated increase in precipitation (Figure 6) acts to reduce salinity at the surface, and ice melt and reduced ice growth (brine rejection) also contribute to freshening. Salinity increases at depth are more likely due to changes in advection by both the meridional and vertical transports.

A combination of the freshening and warming leads to a reduction in density in surface waters globally, and in deep waters generated near the Antarctic coast (Figure 13c). The increase in the temperature of AABW is partially counteracted by the increase in salinity, but not enough to offset it, so its density is still reduced. Surface waters show a maximum decrease in density

of ~ 0.5 kgm^{-3}, with AABW and North Atlantic Deep Water (NADW) decreasing by ~ 0.2 kgm^{-3}. Having less dense water at the surface may reduce upwelling, acting as a stable lid in polar regions.

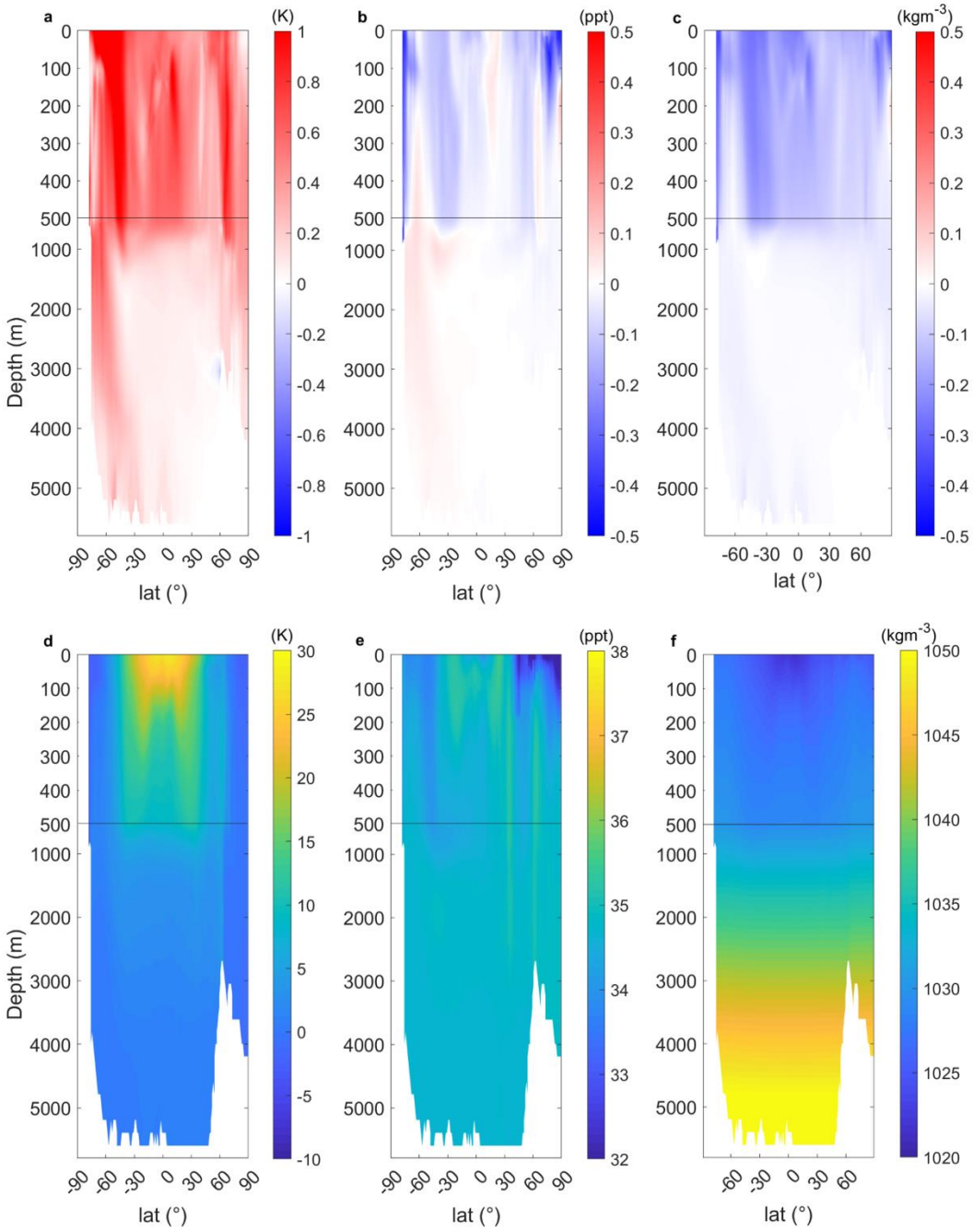

Figure 13. (a) Zonal- and annual-mean potential seawater temperature response, i.e., perturbed minus control. Note that a discontinuous depth axis has been used to highlight the features in the top 500m. (b) As a but for salinity. (c) As a but for density. (d) Zonal- and annual-mean temperature in the coupled control experiment. (e) As d but for salinity. (f) As d but for density.

Vertical temperature-salinity (T-S) profiles are presented in Figure 14 to assess changes to the water column and in characteristic water masses. T-S profiles show how the density of the water changes as a function of potential temperature and salinity. Where density increases with depth, the water column is considered stable, which restricts vertical mixing. Conversely, decreasing density with depth implies an unstable water column, conducive to vertical mixing. Key water masses can be recognized on a T-S diagram by their specific tracer properties. Typically, the bend point identifies the core of the water mass and the lines between the bend points represent mixing between adjacent water masses. Due to the non-linear relationship between temperature and density, temperature change is the dominant driver of density change in warmer waters (visually, this appears in the T-S plot as more tilted isopycnals), whereas salinity change is the dominant driver of density change in colder waters (seen as more vertically aligned isopycnals).

In the Southern Ocean at 70 °S, colder surface waters overlie warmer waters at depth. In the warm season, surface waters above the seasonal thermocline are warmed and freshened by sea-ice loss, leading to a weakened density gradient in the upper layers and thus, a reduced mixed layer depth (Figure 14a). Below the seasonal thermocline in warm season, and throughout the water column in the cold season, water masses remain approximately the same density, despite warming (i.e., the profiles are shifted along isopycnals in Figure 14a,b). Recall that at this latitude, density is controlled by salinity more than temperature (i.e., the isopycnals are nearly vertical).

In the Southern Ocean at 50 °S, the entire water column warms in response to sea-ice loss, year-round, with the biggest increase of 1.5 K at the surface, above the seasonal thermocline (Figure 14c,d). Salinity is reduced in the surface and intermediate waters, again in all seasons. Sea-ice loss results in less dense surface waters in all seasons (warmer and fresher; recall that at this latitude, temperature change dominates over salinity change in the density response), meaning a more stable water column and increased stratification in the upper ocean. Although a year-round increase in both temperature and salinity is found in the Deep Waters and AABW, the density of these waters remains largely the same, and hence the structure of the water column at these depths is unchanged. Therefore, at 50 ° S the greatest changes to density occur toward the top of the water column.

In the tropics, the water column is warmer than at high southern latitudes and thus, changes in temperature are more important than changes in salinity for determining the density response

(note the near-horizontal isopycnals in Figure 14e, f). At the equator, there are smaller differences in salinity or temperature in response to sea-ice loss than in the Southern Ocean. The maximum response in the water column is at the surface, where there is warming of ~1 K and a slight freshening of 0.1. At depth, there is a small decrease in salinity and warming of intermediate waters, but minimal change in Deep Waters. Overall, the profiles show a slight decrease in density in response to sea-ice loss from intermediate levels to the surface.

In the Arctic Ocean at 85 °N, surface and intermediate waters warm by 0.5 K (Figure 14g,h). At greater depth, the response is dominated by changes in salinity (i.e., the curves are shifted horizontally), specifically freshening, likely in response to induced Arctic sea-ice loss. In the Arctic Ocean, density changes are very strongly determined by salinity changes (i.e., near vertical isopycnals) and hence, salinity determines stratification. The vertical density structure of the water column is largely unchanged, but density is reduced at in the upper 500m, which increases the stability of the water column and reduces vertical mixing.

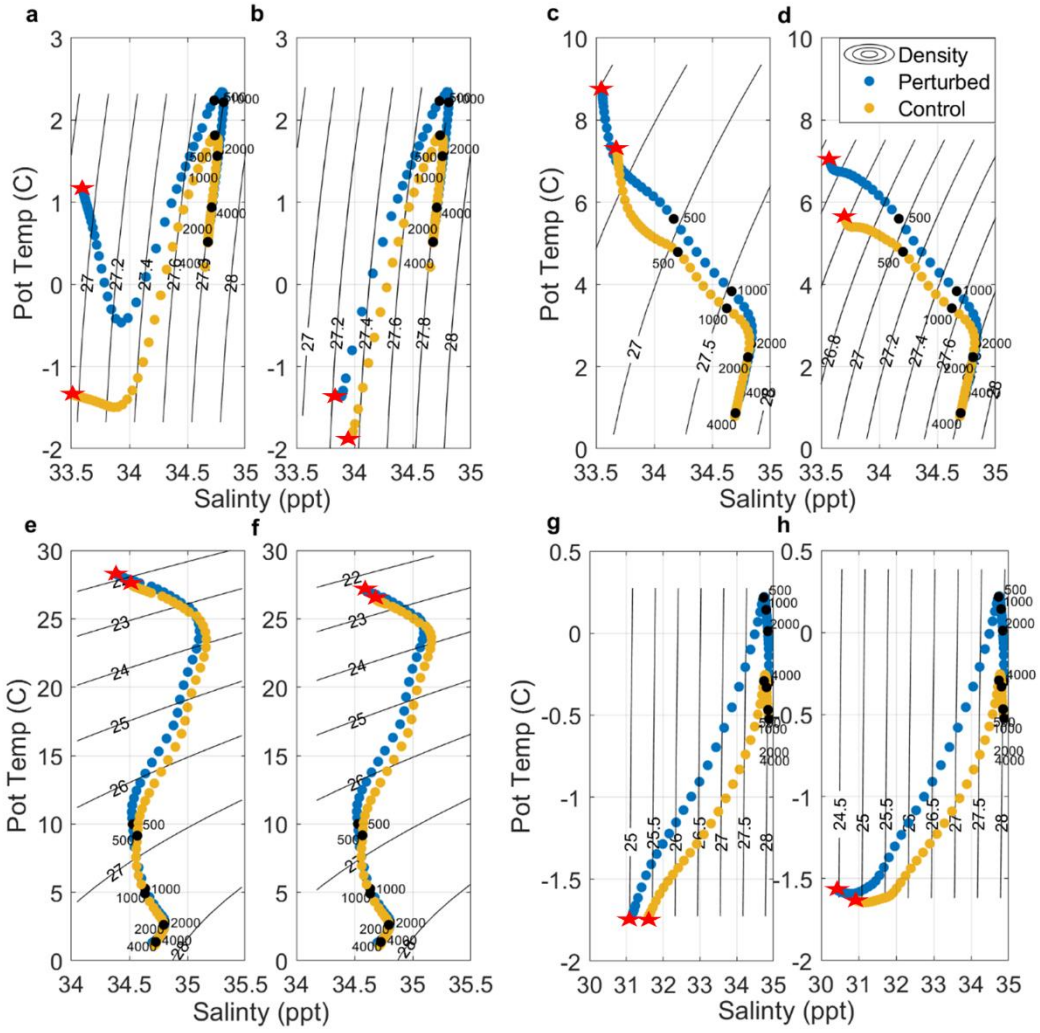

Figure 14. (a) Zonal-mean temperature-salinity profiles at 70 °S for the warm season. Orange dots show the control experiment and blue dots the perturbed experiment. Depth and water density increase from left to right across the figure, red stars denote top of water column. Black curves denote isopycnals, i.e., lines of constant density and the black dots denote depth. (b) As a but for the cold season. (c, d) As a, b but at 50 °S. (e, f) As a, b but at the equator. (g, h) As a, b but at 85 °N.

h. Ocean circulation changes

The zonal-mean zonal velocity in the Southern Ocean is dominated by the Antarctic Circumpolar Current (ACC) and the Antarctic coastal current (Figure 15b), both driven by the wind. In the latitudes of the ACC (~ 40-60 °S), zonal velocity in the upper ocean increases on the southern flank and decreases on the northern flank. With depth, a more consistent decrease in zonal velocity is seen within the ACC. In the tropics, there is a reduction in the equatorial currents.

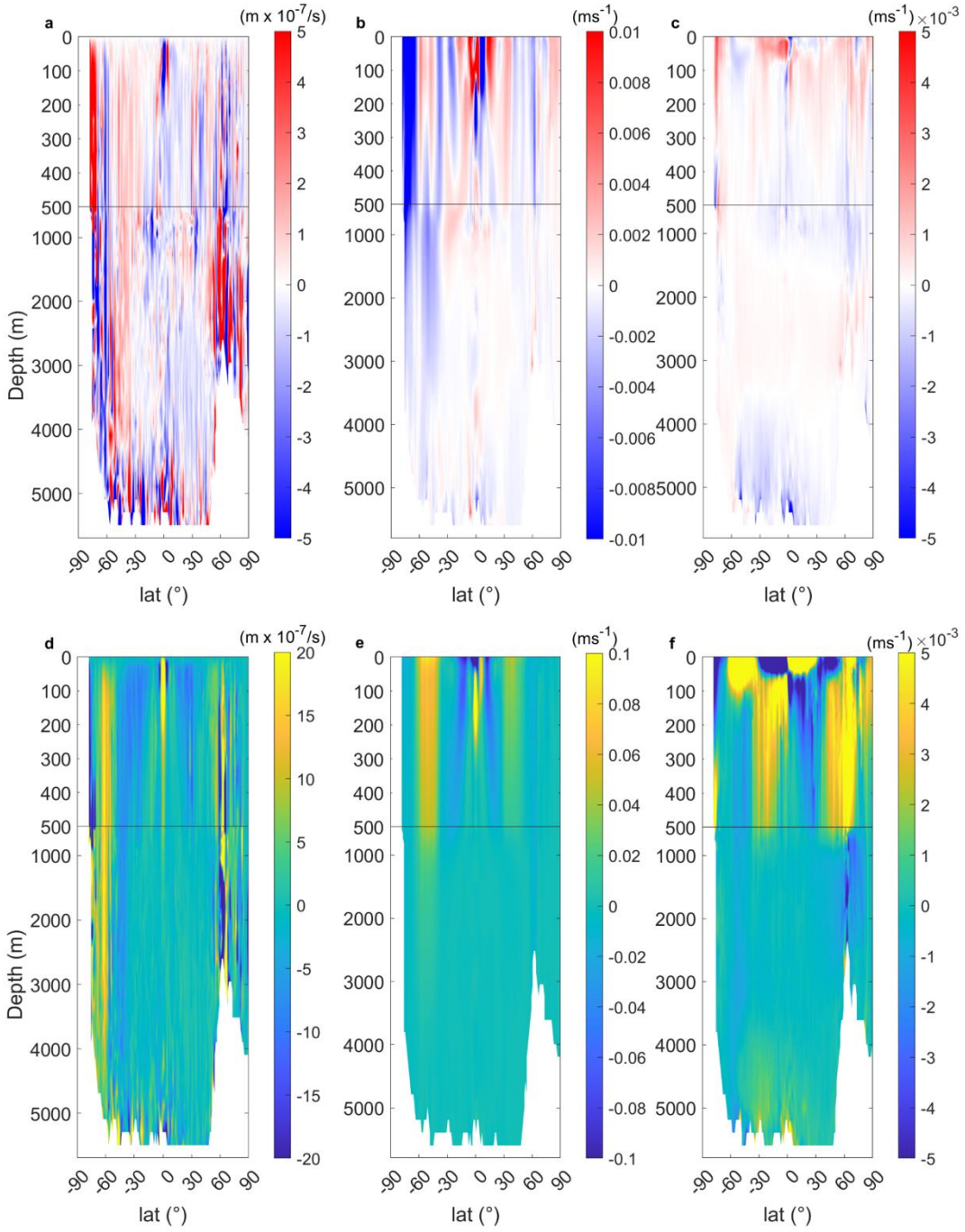

Figure 15. (a) Zonal- and annual-mean vertical velocity response, i.e., perturbed minus control. Note that a discontinuous depth axis has been used to highlight the features in the top 500m. (b) As a but for zonal velocity response. (c) As a but for meridional velocity response. (d) Zonal- and annual-mean vertical velocity in the coupled control experiment. (e) As d but for zonal velocity. (f) As d but for meridional velocity.

Changes in the zonal-mean meridional velocity are small in comparison to the zonal velocity response (Figure 15d). Within the ACC, there is a decrease in northward velocity. At depth (~4000-5000m), the mean northward velocity of Antarctic Bottom Water (AABW) is decreased at latitudes 30 °N – 60 °S. The surface water of the tropics shows a reduced

southward velocity in the Southern Hemisphere (northward response in region of mean southward flow, c.f. Figure 15b,d), and reduced northward velocity in the Northern Hemisphere (southward response in region of mean northward flow, c.f. Figure 15c,f), related to the reduced equatorial upwelling and weakened overturning of the tropical convergence cell (Figure 7). At 2000-4000m depth, the mean southward transport of NADW is slightly reduced in latitudes 40-80 °N (Figure 15 f).

The zonal-mean vertical velocity provides insight into changes in mixing resulting from density and wind driven processes. Throughout the Southern Ocean, downwelling of bottom waters at the very high latitudes off the coastal shelf is reduced (i.e., there is generally an upward velocity response in regions of climatological downwelling, c.f. Figure 15a,d). Also, upwelling of deep waters in latitudes 60-70 °S is reduced (i.e., generally a downward velocity response in regions of climatological upwelling). At lower latitudes of the Southern Ocean, climatological downwelling is reduced by sea-ice loss. Equatorial upwelling of cold water in the tropics is also weakened, as discussed earlier.

A marked decrease in the ACC volume transport of 25-40 Sv is simulated (Figure 16a), but with little seasonal variation (not shown). This is a reduction of 18% compared to the mean ACC transport in the control run (~ 150 Sv). Annual-mean ACC volume transport declines steadily from the beginning of the simulation for about seventy years, and thereafter, fluctuates around a lower mean (~27 Sv), not recovering back to its original state. The decreased ACC transport appears to partially be in response to the weakened overlying zonal wind stress (Figure 16b). Annual-mean zonal wind stress is broadly reduced along the path of the ACC, especially over the Pacific and Indian sectors. Whilst the depth integrated ACC transport through Drake Passage decreases, there is both spatial and vertical variability in the zonal velocity response to sea-ice loss. In the top 500 m, there are filaments of increased and decreased zonal flow within the latitudes of the ACC (Figure 16c). At 500-2000 m depth, a clearer pattern of decreased zonal velocity emerges over the latitudes of the ACC (Figure 16d). A greater depth, below 2000 m, the zonal velocity is broadly decreased, but with lesser magnitude than at intermediate depths (Figure 16e). However, the mean ACC transport at depth is also weaker (Figure 15b).

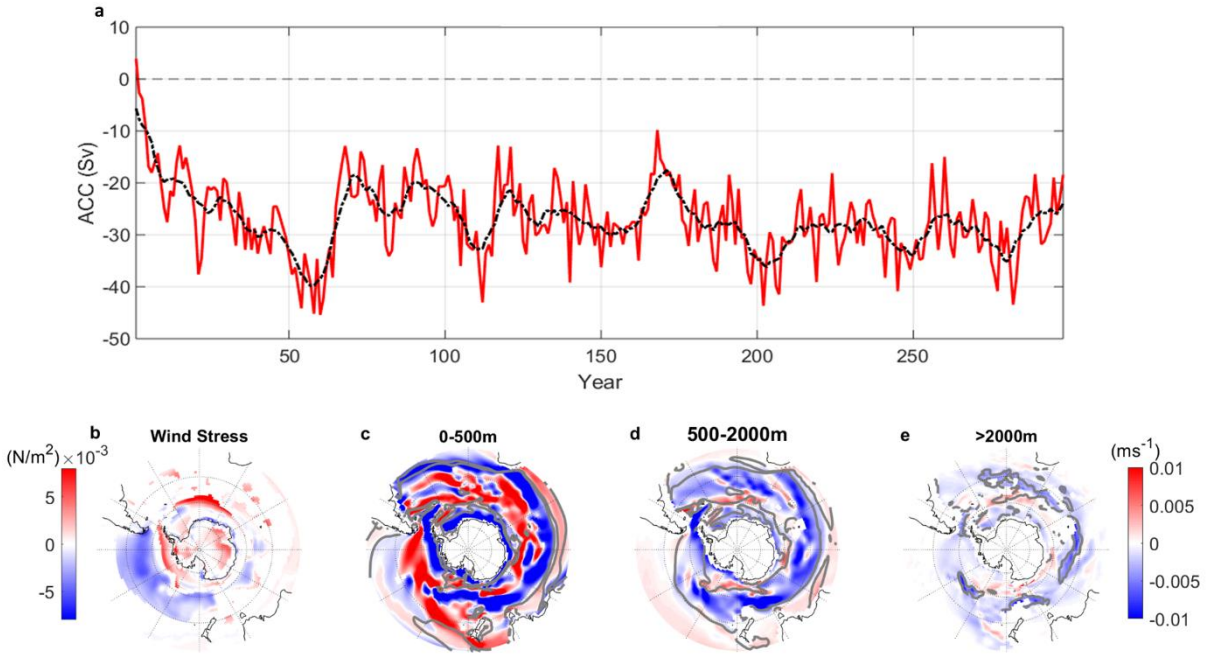

Figure 16. (a) Time-series of annual-mean ACC transport response, i.e., perturbed minus control. The black curve denotes a 10-year running mean. (b) Annual-mean wind stress response. (c) Annual-mean zonal velocity response averaged over the top 500 m. (d) As c but averaged between 500-2000m. (e) As c but averaged below 2000m.

4. Discussion

The results presented suggest an important role for ocean coupling, both in amplifying local changes and in generating far-field responses. The local warming and wetting responses were approximately twice as large in the coupled model as the uncoupled model. This is comparable to Deser et al. (2016), which reported that ocean coupling amplified the warming response to Arctic sea-ice loss by approximately 50%. Warming in the coupled model reached the Antarctic continental interior, but did not in the atmosphere-only model, consistent with England et al. (2018; 2020a; 2020b) that used different climate models and sea ice loss methods. This may be for similar reasons to those proposed in the Arctic (e.g., Blackport & Kushner, 2017), whereby the coupling allows for the surrounding oceans to warm and then warm anomalies are transported along isentropic surfaces (Laliberté and Kushner 2013) from the mid-latitude ocean surface to the high-latitude mid-troposphere. In addition to the 'fast' and largely local responses, the coupled model experiments revealed additional 'slow' and global responses. The coupled model displays a clear "mini-global warming" signature, with warming maxima in the high-latitude lower troposphere and tropical upper-troposphere. The

651 tropical warming, thought to be primarily driven through warmer tropical SSTs and enhanced
652 convection through a weakening of the easterly trade winds, is absent in the atmosphere-only
653 model, strongly suggesting that ocean coupling is vital in communicating Antarctic changes to
654 the rest of the globe. This result is also consistent with England et al. (2020a; 2020b), and
655 echoes the response to Arctic sea-ice loss (e.g Blackport & Kushner, 2016; Deser et al., 2016;
656 Deser et al., 2015; Oudar et al., 2017), which has also been shown to be locally confined in
657 atmospheric-only models but global in reach in coupled models. Globally, the patterns of ocean
658 warming and salinity change with latitude and depth were alike that in response to increased
659 CO_2 (e.g., Collins et al., 2013), but lesser in magnitude. Thus, it is also appropriate to think of
660 the oceanic response to Antarctic sea-ice loss as a 'mini global warming' response, as well as
661 the atmospheric response.

662 Another distinct aspect of the response to Antarctic sea-ice loss, seen in coupled but not in
663 uncoupled experiments, is warming in the Arctic and associated Arctic sea-ice loss, similar to
664 that reported in England et al. (2020b). It is hypothesised that the mechanism for this pole-to-
665 pole connection involves the ocean, as there is an approximate 20-year lag between the initial
666 Antarctic sea-ice loss and the resulting Arctic sea ice response. One possible mechanism is
667 tropical to northern extratropical teleconnections triggered by changes in tropical precipitation
668 (i.e., convection). Antarctic sea-ice loss causes a deepening of the Aleutian Low, observed in
669 the surface pressure response, which may be triggered by a Rossby wave train from the tropical
670 Pacific (e.g. England et al., 2020b; McCrystall et al., 2020; Yuan et al., 2018). Seasonally, the
671 deepening of the Aleutian Low is greatest in boreal winter, when tropical to extratropical
672 teleconnections are known to be most active. The seasonality of this response is also in
673 agreement with England et al. (2020b). Similarly, at high southern latitudes the more
674 pronounced weakening of the Amundsen Sea Low in austral winter (and transitional seasons)
675 is consistent with a Rossby wave train response to the tropical Pacific (Turner, 2004).

676 A significant shift equatorward of the mid-latitude tropospheric eddy-driven jet, leading to
677 a more negative SAM index and most prominent in austral autumn and winter, was simulated
678 in both the coupled and atmospheric-only experiments. Jet strength was weakened during most
679 of the year, but with lesser magnitude in the atmosphere-only model compared to the coupled
680 model. Jet strength is highly dependent on the meridional temperature gradient (and
681 baroclinity), which is decreased more in the coupled model than in the atmosphere-only model.
682 By contrast, the jet shift seems less dependent on the magnitude of high latitude warming. Jet

shifts may be more dependent on the initial position of the jet (Bracegirdle et al. 2018; Simpson et al. 2021). Although the jet response is qualitatively similar to that seen in past studies using atmosphere-only models (Bader et al., 2013; England et al., 2018; Kidston et al., 2011; Menéndez et al., 1999; Raphael et al., 2011; Smith et al., 2017), the lack of ocean coupling in prior studies means it may have been underestimated. The jet response to Antarctic sea-ice loss acts to slightly offset the strengthening and poleward shift of the jet in response to increased CO_2 (e.g., Barnes and Polvani 2013), analogous to the "tug-of-war" on the Northern Hemisphere jet between Arctic sea-ice loss and increased CO_2 (e.g., Deser et al., 2016).

Oceanic responses to Antarctic sea-ice loss included changes to density, temperature, stratification, and mixing, in the Southern Ocean; a reduction in the ACC transport at mid-depths; a weakening of the tropical shallow convergence cell; and freshening of the Arctic Ocean due to Arctic sea-ice loss. The zonally averaged temperature response with depth is similar to that of the atmosphere, and is comparable to a 'mini global warming' response (Collins et al., 2013). ACC transport was reduced by ~20% in the perturbed simulation in comparison to the control, consistent with reduced surface wind stress due to a weakening of the tropospheric eddy-driven jet. The reverse - a small increase in ACC transport in response to increased sea ice and a strengthened westerly jet - was found by Downes et al. (2011). However, the effect of changes in westerly jet strength on the ACC is still a matter of some debate (e.g., Böning et al., 2008; Farneti & Delworth, 2010; Farneti et al., 2010; Hallberg and Gnanadesikan, 2006). Shi et al. (2021) found an increase in ACC transport in response to Southern Ocean warming, noting that the wind stress had a secondary role to temperature. That our simulations show a reduction in ACC transport despite Southern Ocean warming, further points to a key role for reduced wind stress and/or increased salinity at the shelf. A possible limitation of the low resolution HadGEM3-GC3.1-LL model is that it parametrizes the effects of mesoscale eddies. It is plausible that a different ACC response to sea-ice loss would have been obtained if the model resolved eddies (e.g., Munday et al., 2013), albeit the response is broadly consistent (but opposite in sign) to Downes et al. (2010), that used an eddy-permitting model.

5. Summary and Conclusions

The climate impacts of Antarctic sea-ice loss have not been researched to the same extent as the impacts of Arctic sea-ice loss**.** This study was one of the first to assess the coupled climate response to Antarctic sea-ice loss, which can be summarised as follows. Abrupt Antarctic sea-ice loss immediately caused an enhanced heat flux from ocean to atmosphere, triggering localised tropospheric warming and wetting. Strong warming and freshening of surface waters in the Southern Ocean led to a more stratified and stable water column. The equator-to-pole temperature gradient was reduced, and thus, the tropospheric eddy-driven jet was weakened, projecting onto the negative SAM phase. Weakened surface wind stress contributed to a 20% reduction in the ACC transport, and reduced the northward Ekman transport of cold water, further warming the upper Southern Ocean. Warmed Southern Ocean SSTs allowed the atmosphere warming to spread from the Southern midlatitudes to the Antarctic plateau by advection; supported by the absence of such continental warming in uncoupled experiments. Over several decades, ocean surface warming reached the tropics. Here, reduced easterly equatorial winds led to a weakened upper ocean tropical convergence cell, and reduced upwelling of cold water, further enhancing the surface warming. Warmer tropical SSTs may have enhanced convection and drove upper tropospheric warming, triggering anomalous teleconnections into the extratropics, for example, strengthening the Aleutian Low. Further supporting a key role for ocean coupling, analogous uncoupled experiments yielded an atmospheric response much more locally confined compared to that in the coupled model. Twenty to fifty years later in the coupled runs, after the abrupt loss of Antarctic sea-ice, warming reached the Arctic, triggering Northern Hemisphere sea-ice loss and thereby, near-surface warming and freshening of the Arctic Ocean. Both the atmospheric and oceanic responses are much like those projected for scenarios of increased greenhouse gases, but with lesser magnitude.

Acknowledgments.

We thank Katy Sheen and Julie Jones for their valuable discussion and comments on results included in this paper. We also thank Leon Hermanson and Rosie Eade for contribution to the ensemble models. PiControl Met Office HadGEM3-GC31-LL data was obtained from the Earth System Grid Federation and Centre for Environmental Data Analysis, submitted as part of the Climate Model Intercomparison Project Phase 6. This study was supported by the "Robust Spatial Projections of Real-World Climate Change" (NERC, Research grant

NE/N018486/1) and the University of Exeter. EB and the development of the HadGEM3-GC31 climate model were supported by the Met Office Hadley Centre Climate Programme funded by BEIS.

Data Availability Statement.

The numerical model simulations upon which this study arises based are too large to archive in full. Requests for selected output should be sent to the corresponding author. The coupled control simulation can be found via the Earth Earth System Grid Federation and Centre for Environmental Data Analysis submitted as part of the Climate Model Intercomparison Project Phase 6.

REFERENCES

Andrews, M. B., and Coauthors, 2020: Historical Simulations With HadGEM3-GC3.1 for CMIP6. J. Adv. Model. Earth Syst., 12, 1–34, https://doi.org/10.1029/2019MS001995

Ayres, H. C., and J. A. Screen, 2019: Multimodel Analysis of the Atmospheric Response to Antarctic Sea Ice Loss at Quadrupled CO2. Geophys. Res. Lett., 46, 9861–9869, https://doi.org/10.1029/2019GL083653.

Bader, J., M. Flügge, N. G. Kvamstø, M. D. S. Mesquita, and A. Voigt, 2013: Atmospheric winter response to a projected future Antarctic sea-ice reduction: A dynamical analysis. Clim. Dyn., 40, 2707–2718, https://doi.org/10.1007/s00382-012-1507-9.

Barnes, E. A., and L. M. Polvani, 2013: Response of the Midlatitude Jets, and of Their Variability, to Increased Greenhouse Gases in the CMIP5 Models. J. Clim., 26, 7117–7135, https://doi.org/https://doi.org/10.1175/JCLI-D-12-00536.1.

Bintanja, R., G. J. Van Oldenborgh, S. S. Drijfhout, B. Wouters, and C. A. Katsman, 2013: Important role for ocean warming and increased ice-shelf melt in Antarctic sea-ice expansion. Nat. Geosci., 6, 376–379, https://doi.org/10.1038/ngeo1767.

Blackport, R., and P. J. Kushner, 2016: The transient and equilibrium climate response to rapid summertime sea ice loss in CCSM4. J. Clim., 29, 401–417, https://doi.org/10.1175/JCLI-D-15-0284.1.

Blackport, R., and P. J. Kushner, 2017: Isolating the atmospheric circulation response to arctic sea ice loss in the coupled climate system. J. Clim., 30, 2163–2185, https://doi.org/10.1175/JCLI-D-16-0257.1.

775 Blackport, R., & Screen, J. A. (2020). Insignificant effect of arctic amplification on the
776 amplitude of midlatitude atmospheric waves. Science Advances, 6(8), 277–286.eaay2880.
777 https://doi.org/10.1126/sciadv.aay2880

778 Böning, C. W., A. Dispert, M. Visbeck, S. R. Rintoul, and F. U. Schwarzkopf, 2008: The
779 response of the antarctic circumpolar current to recent climate change. Nat. Geosci., 1,
780 864–869, https://doi.org/10.1038/ngeo362.

781 Bracegirdle, T. J., P. Hyder, and C. R. Holmes, 2018: CMIP5 Diversity in Southern Westerly
782 Jet Projections Related to Historical Sea Ice Area: Strong Link to Strengthening and
783 Weak Link to Shift. J. Clim., 31, 195–211, https://doi.org/10.1175/JCLI-D-17-0320.1.

784 Briegleb, B. P., and B. Light, 2007: A Delta-Eddington Multiple Scattering Parameterization
785 for Solar Radiation in the Sea Ice Component of the Community Climate System Model.
786 100 pp.

787 Ceppi, P., G. Zappa, T. G. Shepherd, and J. M. Gregory, 2017: Fast and slow components of
788 the extratropical atmospheric circulation response to CO 2 forcing. J. Clim., 31, 1091–
789 1105, https://doi.org/10.1175/JCLI-D-17-0323.1.

790 Cohen, J., and Coauthors, 2014: Recent Arctic amplification and extreme mid-latitude
791 weather. Nat. Geosci., 7, 627–637, https://doi.org/10.1038/ngeo2234.

792 Collins, M., and Coauthors, 2013: Long-term Climate Change: Projections, Commitments
793 and Irreversibility. Clim. Chang. 2013 Phys. Sci. Basis. Contrib. Work. Gr. I to Fifth
794 Assess. Rep. Intergov. Panel Clim. Chang., 1029–1136,
795 https://doi.org/10.1017/CBO9781107415324.024.

796 Deser, C., R. A. Tomas, and L. Sun, 2015: The role of ocean-atmosphere coupling in the
797 zonal-mean atmospheric response to Arctic sea ice loss. J. Clim., 28, 2168–2186,
798 https://doi.org/10.1175/JCLI-D-14-00325.1.

799 Deser, C., L. Sun, R. A. Tomas, and J. Screen, 2016: Does ocean coupling matter for the
800 northern extratropical response to projected Arctic sea ice loss? Geophys. Res. Lett., 43,
801 2149–2157, https://doi.org/10.1002/2016GL067792.

802 Downes, S. M., N. L. Bindoff, and S. R. Rintoul, 2010: Changes in the subduction of
803 Southern Ocean water masses at the end of the twenty-first century in eight IPCC models.
804 J. Clim., 23, 6526–6541, https://doi.org/10.1175/2010JCLI3620.1.

805 Downes, S. M., A. S. Budnick, J. L. Sarmiento, and R. Farneti, 2011: Impacts of wind stress
806 on the Antarctic Circumpolar Current fronts and associated subduction. Geophys. Res.
807 Lett., 38, 3–8, https://doi.org/10.1029/2011GL047668.

808 Eayrs, C., X. Li, M. N. Raphael, and D. M. Holland, 2021: Rapid decline in Antarctic sea ice
809 in recent years hints at future change. Nat. Geosci., 14, 460–464,
810 https://doi.org/10.1038/s41561-021-00768-3.

811 England, M., L. Polvani, and L. Sun, 2018: Contrasting the Antarctic and Arctic atmospheric
812 responses to projected sea ice loss in the late twenty-first century. J. Clim., 31, 6353–
813 6370, https://doi.org/10.1175/JCLI-D-17-0666.1.

814 England, M. R., L. M. Polvani, and L. Sun, 2020a: Robust Arctic warming caused by
815 projected Antarctic sea ice loss. Environ. Res. Lett., in press, 0–31,
816 https://doi.org/10.1088/1748-9326/abaada.

817 England, M. R., L. M. Polvani, L. Sun, and C. Deser, 2020b: Tropical climate responses to
818 projected Arctic and Antarctic sea-ice loss. Nat. Geosci., 13, 275–281,
819 https://doi.org/10.1038/s41561-020-0546-9.

820 Eyring, V., S. Bony, G. A. Meehl, C. A. Senior, B. Stevens, R. J. Stouffer, and K. E. Taylor,
821 2016: Overview of the Coupled Model Intercomparison Project Phase 6 (CMIP6)
822 experimental design and organization. Geosci. Model Dev., 9, 1937–1958,
823 https://doi.org/10.5194/gmd-9-1937-2016.

824 Farneti, R., and T. L. Delworth, 2010: The role of mesoscale eddies in the remote oceanic
825 response to altered Southern Hemisphere winds. J. Phys. Oceanogr., 40, 2348–2354,
826 https://doi.org/10.1175/2010JPO4480.1.

827 Farneti, R., and T. L. Delworth, 2010, A. J. Rosati, S. M. Griffies, and F. Zeng, 2010: The
828 role of mesoscale eddies in the rectification of the Southern Ocean response to climate
829 change. J. Phys. Oceanogr., 40, 1539–1557,
830 https://doi.org/10.1175/2010JPO4353.1.Flocco, D., D. L. Feltham, and A. K. Turner,
831 2010: Incorporation of a physically based melt pond scheme into the sea ice component
832 of a climate model. J. Geophys. Res. Ocean., 115, 1–14,
833 https://doi.org/10.1029/2009JC005568.

834 Hunke, E. C., W. H. Lipscomb, A. K Turner, N. Jeffery and S. Elliott. 2015: CICE: the Los
835 Alamos Sea ice Model Documentation and Software User's Manual Version 5.1, LA-
836 CC-06-012, Los Alamos National Laboratory, Los Alamos, NM, 2015.

837 Kidston, J., A. S. Taschetto, D. W. J. Thompson, and M. H. England, 2011: The influence of
838 Southern Hemisphere sea-ice extent on the latitude of the mid-latitude jet stream.
839 Geophys. Res. Lett., 38, 1–5, https://doi.org/10.1029/2011GL048056.

840 Kim, B. M., S. W. Son, S. K. Min, J. H. Jeong, S. J. Kim, X. Zhang, T. Shim, and J. H. Yoon,
841 2014: Weakening of the stratospheric polar vortex by Arctic sea-ice loss. Nat. Commun.,
842 5, 1–8, https://doi.org/10.1038/ncomms5646.

843 Kuhlbrodt, T., and Coauthors, 2018: The Low-Resolution Version of HadGEM3 GC3.1:
844 Development and Evaluation for Global Climate. J. Adv. Model. Earth Syst., 10, 2865–
845 2888, https://doi.org/10.1029/2018MS001370.

846 Laliberté, F., and P. J. Kushner, 2013: Isentropic constraints by midlatitude surface warming
847 on the Arctic midtroposphere. Geophys. Res. Lett., 40, 606–611,
848 https://doi.org/10.1029/2012GL054306.

849 Liu, J., and J. A. Curry, 2010: Accelerated warming of the Southern Ocean and its impacts on
850 the hydrological cycle and sea ice. Proc. Natl. Acad. Sci. U. S. A., 107, 14987–14992,
851 https://doi.org/10.1073/pnas.1003336107.

852 Ludescher, J., N. Yuan, and A. Bunde, 2018: Detecting the statistical significance of the
853 trends in the Antarctic sea ice extent: an indication for a turning point. Clim. Dyn., 53,
854 237–244, https://doi.org/10.1007/s00382-018-4579-3.

855 Mackie, S., I. J. Smith, J. K. Ridley, D. P. Stevens, and P. J. Langhorne, 2020: Climate
856 response to increasing antarctic iceberg and ice shelf melt. J. Clim., 33, 8917–8938,
857 https://doi.org/10.1175/JCLI-D-19-0881.1.

858 McCrystall, M. R., J. S. Hosking, I. P. White, and A. C. Maycock, 2020: The Impact of
859 Changes in Tropical Sea Surface Temperatures over 1979–2012 on Northern Hemisphere
860 High-Latitude Climate. J. Clim., 33, 5103–5121, https://doi.org/10.1175/jcli-d-19-0456.1.

861 Meehl, G. A., J. M. Arblaster, C. T. Y. Chung, M. M. Holland, A. DuVivier, L. Thompson,
862 D. Yang, and C. M. Bitz, 2019: Sustained ocean changes contributed to sudden Antarctic

sea ice retreat in late 2016. Nat. Commun., 10, 14, https://doi.org/10.1038/s41467-018-07865-9.

Menary, M. B., and Coauthors, 2018: Preindustrial Control Simulations With HadGEM3-GC3.1 for CMIP6. J. Adv. Model. Earth Syst., 10, 3049–3075, https://doi.org/10.1029/2018MS001495.

Menéndez, C. G., V. Serafini, and H. Le Treut, 1999: The effect of sea-ice on the transient atmospheric eddies of the Southern Hemisphere. Clim. Dyn., 15, 659–671, https://doi.org/10.1007/s003820050308.

Meredith, M., M. Sommerkorn, S. Cassotta, C. Derksen, A. Ekaykin, A. Hollowed, G. Kofinas, A. Mackintosh, J. Melbourne-Thomas, M.M.C. Muelbert, G. Ottersen, H. Pritchard, and E.A.G. Schuur, 2019: Polar Regions. In: IPCC Special Report on the Ocean and Cryosphere in a Changing Climate. IPCC, 3, S129–S131, https://doi.org/10.1016/S1366-7017(01)00066-6.

Munday, D. R., H. L. Johnson, and D. P. Marshall, 2013: Eddy saturation of equilibrated circumpolar currents. J. Phys. Oceanogr., 43, 507–532, https://doi.org/10.1175/JPO-D-12-095.1.

Oudar, T., E. Sanchez-Gomez, F. Chauvin, J. Cattiaux, L. Terray, and C. Cassou, 2017: Respective roles of direct GHG radiative forcing and induced Arctic sea ice loss on the Northern Hemisphere atmospheric circulation. Clim. Dyn., 0, 1–21, https://doi.org/10.1007/s00382-017-3541-0.

Parkinson, C. L., 2019: A 40-y record reveals gradual Antarctic sea ice increases followed by decreases at rates far exceeding the rates seen in the Arctic. Proc. Natl. Acad. Sci., 201906556, https://doi.org/10.1073/pnas.1906556116.

Peings, Y., and G. Magnusdottir, 2014: Response of the wintertime northern hemisphere atmospheric circulation to current and projected arctic sea ice decline: A numerical study with CAM5. J. Clim., 27, 244–264, https://doi.org/10.1175/JCLI-D-13-00272.1.

Polvani, L. M., D. W. Waugh, G. J. P. Correa, and S. W. Son, 2011: Stratospheric ozone depletion: The main driver of twentieth-century atmospheric circulation changes in the Southern Hemisphere. J. Clim., 24, 795–812, https://doi.org/10.1175/2010JCLI3772.1.

892 Hallberg, R., and A. Gnanadesikan, 2006: The Role of Eddies in Determining the Structure
893 and Response of the Wind-Driven Southern Hemisphere Overturning: Results from the
894 Modeling Eddies in the Southern Ocean (MESO) Project. J. Phys. Oceanogr., 36, 2232–
895 2252.

896 Raphael, M. N., W. Hobbs, and I. Wainer, 2011: The effect of Antarctic sea ice on the
897 Southern Hemisphere atmosphere during the southern summer. Clim. Dyn., 36, 1403–
898 1417, https://doi.org/10.1007/s00382-010-0892-1.

899 Raphael, M.N., and M.S. Handcock, 2022: A new record minimum for Antarctic sea ice. Nat
900 Rev Earth Environ . https://doi.org/10.1038/s43017-022-00281-0

901 Ridley, J. K., E. W. Blockley, A. B. Keen, J. G. L. Rae, A. E. West, and D. Schroeder, 2018:
902 The sea ice model component of HadGEM3-GC3.1. Geosci. Model Dev., 11, 713–723,
903 https://doi.org/10.5194/gmd-11-713-2018.

904 Roach, L. A., and Coauthors, 2020: Antarctic Sea Ice Area in CMIP6. Geophys. Res. Lett.,
905 47, 1–10, https://doi.org/10.1029/2019GL086729.

906 Schlosser, E., F. A. Haumann, M. N. Raphael, F. Alexander Haumann, and M. N. Raphael,
907 2017: Atmospheric influences on the anomalous 2016 Antarctic sea ice decay. Cryosph.
908 Discuss., 13, 1–31, https://doi.org/10.5194/tc-2017-192.

909 Scott, F., and D. L. Feltham, 2010: A model of the three-dimensional evolution of Arctic melt
910 ponds on first-year and multiyear sea ice. J. Geophys. Res. Ocean., 115, 1–37,
911 https://doi.org/10.1029/2010JC006156.

912 Screen, J. A., and I. Simmonds, 2013: Exploring links between Arctic amplification and mid-
913 latitude weather. Geophys. Res. Lett., 40, 959–964, https://doi.org/10.1002/grl.50174.

914 Screen, J. A., and I. Simmonds, C. Deser, and R. Tomas, 2013: The atmospheric response to
915 three decades of observed arctic sea ice loss. J. Clim., 26, 1230–1248,
916 https://doi.org/10.1175/JCLI-D-12-00063.1.

917 Screen, J. A., and Coauthors, 2018a: Consistency and discrepancy in the atmospheric
918 response to Arctic sea-ice loss across climate models. Nat. Geosci., 11, 155–163,
919 https://doi.org/10.1038/s41561-018-0059-y.

Screen, J. A., T. J. Bracegirdle, and I. Simmonds, 2018b: Polar Climate Change as Manifest in Atmospheric Circulation. Curr. Clim. Chang. Reports, 4, 383–395, https://doi.org/10.1007/s40641-018-0111-4.

Shi, J. R., L. D. Talley, S. P. Xie, Q. Peng, and W. Liu, 2021: Ocean warming and accelerating Southern Ocean zonal flow. Nat. Clim. Chang., 11, 1090–1097, https://doi.org/10.1038/s41558-021-01212-5.

Simpson, I. R., K. A. McKinnon, F. V. Davenport, M. Tingley, F. Lehner, A. Al Fahad, and D. Chen, 2021: Emergent constraints on the large-scale atmospheric circulation and regional hydroclimate: Do they still work in CMIP6 and how much can they actually constrain the future? J. Clim., 34, 6355–6377, https://doi.org/10.1175/JCLI-D-21-0055.1.

Singh, H. A., L. M. Polvani, and P. J. Rasch, 2019: Antarctic Sea Ice Expansion, Driven by Internal Variability , in the Presence of Increasing Atmospheric. https://doi.org/10.1029/2019GL083758.

Smith, D. M., N. J. Dunstone, A. A. Scaife, E. K. Fiedler, D. Copsey, and S. C. Hardiman, 2017: Atmospheric response to Arctic and Antarctic sea ice: The importance of ocean-atmosphere coupling and the background state. J. Clim., 30, 4547–4565, https://doi.org/10.1175/JCLI-D-16-0564.1.

Smith, D. M., and Coauthors, 2018: The Polar Amplification Model Intercomparison Project (PAMIP) contribution to CMIP6: investigating the causes and consequences of polar amplification. Geosci. Model Dev. Discuss., 1–42, https://doi.org/10.5194/gmd-2018-82.

Storkey, D., and Coauthors, 2018: UK Global Ocean GO6 and GO7: A traceable hierarchy of model resolutions. Geosci. Model Dev., 11, 3187–3213, https://doi.org/10.5194/gmd-11-3187-2018.

Stuecker, M. F., C. M. Bitz, and K. C. Armour, 2017: Conditions leading to the unprecedented low Antarctic sea ice extent during the 2016 austral spring season. Geophys. Res. Lett., 1–12, https://doi.org/10.1002/2017GL074691.

Sun, L., C. Deser, R. A. Tomas, and M. Alexander, 2020: Global Coupled Climate Response to Polar Sea Ice Loss: Evaluating the Effectiveness of Different Ice-Constraining Approaches. Geophys. Res. Lett., 47, https://doi.org/10.1029/2019GL085788..

949 Taylor, K. E., R. J. Stouffer, and G. A. Meehl, 2012: An overview of CMIP5 and the
950 experiment design. Bull. Am. Meteorol. Soc., 93, 485–498,
951 https://doi.org/10.1175/BAMS-D-11-00094.1.

952 Tomas, R. A., C. Deser, and L. Sun, 2016: The role of ocean heat transport in the global
953 climate response to projected arctic sea ice loss. J. Clim., 29, 6841–6859,
954 https://doi.org/10.1175/JCLI-D-15-0651.1.

955 Turner, J., 2004: The El Niño-Southern Oscillation and Antarctica. Int. J. Climatol., 24, 1–31,
956 https://doi.org/10.1002/joc.965.

957 Turner, J., and Coauthors, 2009: Non-annular atmospheric circulation change induced by
958 stratospheric ozone depletion and its role in the recent increase of Antarctic sea ice extent.
959 Geophys. Res. Lett., 36, 1–5, https://doi.org/10.1029/2009GL037524.

960 Turner, J., T. Phillips, G. J. Marshall, J. S. Hosking, J. O. Pope, T. J. Bracegirdle, and P.
961 Deb, 2017: Unprecedented springtime retreat of Antarctic sea ice in 2016. Geophys. Res.
962 Lett., 44, 6868–6875, https://doi.org/10.1002/2017GL073656.

963 Turner, J., and Coauthors, 2020: Recent Decrease of Summer Sea Ice in the Weddell Sea,
964 Antarctica. Geophys. Res. Lett., 47, https://doi.org/10.1029/2020GL087127.

965 Vavrus, S. J., 2018: The Influence of Arctic Amplification on Mid-latitude Weather and
966 Climate. Curr. Clim. Chang. Reports, 4, 238–249, https://doi.org/10.1007/s40641-018-
967 0105-2.

968 Walters, D., and Coauthors, 2017: The Met Office Unified Model Global Atmosphere 7.0/7.1
969 and JULES Global Land 7.0 configurations. Geosci. Model Dev., 12, 1909–1963,
970 https://doi.org/10.5194/gmd-12-1909-2019.

971 Wang, Z., J. Turner, Y. Wu, and C. Liu, 2019: Rapid decline of total Antarctic sea ice extent
972 during 2014–16 controlled by wind-driven sea ice drift. J. Clim., 32, 5381–5395,
973 https://doi.org/10.1175/JCLI-D-18-0635.1.

974 Williams, K. D., and Coauthors, 2017: The Met Office Global Coupled Model 3.0 and 3.1
975 (GC3.0 and GC3.1) Configurations. J. Adv. Model. Earth Syst., 10, 357–380,
976 https://doi.org/10.1002/2017MS001115.

977 Yuan, X., M. R. Kaplan, and M. A. Cane, 2018: The interconnected global climate system-a
978 review of tropical-polar teleconnections. J. Clim., 31, 5765–5792,
979 https://doi.org/10.1175/JCLI-D-16-0637.1.

980 Zappa, G., F. Pithan, and T. G. Shepherd, 2018a: Multimodel Evidence for an Atmospheric
981 Circulation Response to Arctic Sea Ice Loss in the CMIP5 Future Projections. Geophys.
982 Res. Lett., 45, 1011–1019, https://doi.org/10.1002/2017GL076096.